2020-02-15

New constraints on bedrock erodibility and landscape response times upstream of an active fault

Zondervan, JR

10.1016/j.geomorph.2019.106937
Geomorphology
Elsevier BV

New constraints on bedrock erodibility and landscape response times upstream of an active fault

Jesse R. Zondervan[1,2*], Alexander C. Whittaker[1], Rebecca E. Bell[1], Stephen E. Watkins[1,3], Sam A.S. Brooke[1,4], Madeleine G. Hann[1,5]

(1) Department of Earth Science & Engineering, Imperial College, South Kensington, London SW7 2AZ, UK
(2) Now at: School of Geography, Earth and Environmental Sciences, University of Plymouth, Plymouth, PL4 8AA, UK
(3) Now at: Département des Sciences de la Terre, Université de Genève, Rue des Maraîchers 13, 1205 Genève, Switzerland
(4) Now at: Department of Geography, University of California Santa Barbara, Santa Barbara, California, U.S.A.
(5) Now at: Geography, School of Environment, Education and Development, The University of Manchester, Manchester M13 9PL, UK

Correspondence to: Jesse R. Zondervan (jesse.zondervan@plymouth.ac.uk)

Abstract. Considerable progress has been made in modelling the response of rivers to tectonic perturbation in order to decode the tectonic signals embedded in river long profiles and planform geometry. Whilst studies have showed the importance of rock type on the morphology of rivers responding to tectonics on a local scale, these effects are often not captured in landscape evolution models. In fact, current models of fluvial response to tectonic perturbation such as active faulting require carefully collected data sets to fully constrain or calibrate key parameters, including the effect of bedrock lithology on substrate erodibility and timescales for tectonic signal propagation in bedrock river systems. Here we constrain the role of bedrock in controlling fluvial incision for a 240 km^2 catchment draining into the Gulf of Corinth, which has excellent tectonic constraints and a variety of bedrock lithologies. An active normal fault at the downstream end of the catchment (the East Eliki Fault) is known to have initiated at 0.7 Ma, with average Quaternary uplift and incision rates of 1.00-1.25 mm/yr. The initiation of the East Eliki Fault is recorded in the river as a prominent knickzone 7-16 km upstream of the fault. Detailed field data collected within this catchment at 500 m intervals along the main channel length at this tectonically well-constrained field site show an order of magnitude increase in river channel slopes (y/x = 0.02 to 0.18) and

stream powers (1 kWm^{-2} to 27 kWm^{-2}) at the lithological boundary between weak and resistant bedrock. The weak conglomerates and strong limestones have Schmidt hammer compressive strengths of ca. 30 and 50 respectively, based on in-situ rock strength measurements. Consequent erodibility values of $1.8 \pm 0.3 \times 10^{-14}$ and $5 - 6 \pm 2 \times 10^{-15}$ ms^2kg^{-1} show a factor of three to four decrease in erodibility for a two-fold increase in rock strength. A simple simulation of tectonic signal propagation through the river catchment based on these erodibility values indicates that the observed plan view position of the knickpoint is consistent with our calculated knickpoint positions based on erodibility values derived from incision rate and stream power data. However, the tectonic signal associated with faulting would have propagated completely through the catchment within 1 Ma if it were entirely composed of weak rock for similar climatic and tectonic conditions, indicating that lithology has a major control on landscape response times. Our results help constrain the effect of lithology on river channel geometry and allow erosional parameters to be derived that are crucial for effective modelling of tectonic rates from topography.

Keywords: fluvial erosion, neotectonics, Corinth Rift, bedrock lithology

1 Introduction

Fluvial erosion processes transmit tectonic and climatic signals to the landscape (Wobus et al., 2006; Brocklehurst, 2010). Considerable progress has been made in modelling the transient dynamics of river systems to tectonic perturbation using Digital Elevation Models (DEMs) and numerical models to evaluate the extent to which tectonic signals are embedded in channel long profiles (Tucker et al., 2001; Crosby and Whipple, 2006; Attal et al., 2008; Tucker, 2009). It is widely accepted that detachment-limited (i.e. bedrock) rivers can embed signals of an increased rate of active faulting in their channel long profiles in the form of convex reaches called knickzones, which propagate upstream through the catchment over time (Whipple and Tucker, 1999; Crosby and Whipple, 2006; Whittaker et al., 2008; Kirby and Whipple, 2012; Campforts and Govers, 2015). The timescales at which these knickzones propagate upstream have been shown from both theoretical and empirical perspectives to depend on drainage area and climate (Tucker and Whipple, 2002; Bishop et al., 2005; Berlin and Anderson, 2007; Jansen et al., 2011; Whittaker and Boulton, 2012). These studies have shown that the celerity, or wave speed of a knickpoint migrating upstream, varies as a power-law function of upstream drainage area and is additionally dependent on precipitation rate and potentially sediment input (Cowie et al., 2008). However, the strength of bedrock exposed at the surface should also exert an important control on fluvial dynamics (Stock and

Montgomery, 1999; Wohl and Merritt, 2001; Bursztyn et al., 2015; Forte et al., 2016; Yanites et al., 2017), and should influence the rate at which rivers can incise in response to active faulting (Whipple and Tucker, 2002; Cook et al., 2009; Whittaker and Boulton, 2012; Kent et al., 2017). Nevertheless, while studies have shown the importance of rock type on the morphology of rivers on a local scale (Wohl and Merritt, 2001; Hurst et al., 2013; Chittenden et al., 2014), the results of studies attempting to constrain the effect of bedrock lithology on river response to tectonic perturbation over longer timescales (10^4 to 10^6 years) have been mixed. For example, combining constraints on incision rates, long profiles and modelling, Cook et al. (2009) showed that the knickpoint of the Grand Canyon represents a migrating wave of incision that is likely modulated by differences in rock strength. Similarly, DiBiase et al. (2018) recently showed that a resistant caprock in the Appalachians serves as the boundary between remnant and adjusted topography in this area although the timing and magnitude of the base-level fall was not fully constrained. In contrast, Whittaker and Boulton (2012) were unable to show a clear dependence of knickpoint retreat rates on lithological bedrock strength in tectonically well-constrained bedrock catchments in the Hatay Graben, Turkey, and the Central Apennines, Italy, although their Italian examples displayed limited lithological variability at the catchment scale. Similarly, Kent et al. (2017) demonstrated that knickpoint migration rates differed in a range of catchments crossing active normal faults in the Gediz Graben of Turkey with differing bedrock lithologies, but as this study did not link mapped lithologies to rock strength explicitly, the authors were unable to isolate the effect unequivocally. In addition to these field studies, numerical modelling work suggests that dipping bedrock with varying erodibility can lead to complicated feedbacks between base level, erosion rate, and topography resulting in spatio-temporal variations in erosion rates through a landscape and varying degrees of knickzone expression (Forte et al., 2016; Perne et al., 2017; Yanites et al., 2017). Roy et al. (2015) found, using the landscape evolution model CHILD, that modelled knickpoint migration was faster in a lithologically variable landscape, whilst lithological variation could also 'smear out' knickpoint signals (Forte et al., 2016; Yanites et al., 2017; DiBiase et al., 2018) or refresh them (Yanites et al., 2017).

Consequently, while theory and numerical models predict a role for bedrock erodibility in modulating fluvial responses to relative base-level change, there are very few field data sets that unequivocally demonstrate this. Indeed, the challenge of turning observations and measurements of rock type and strength into workable estimates of bedrock erodibility remains a key problem (e.g. Bursztyn et al., 2015). Addressing this question requires carefully-collected observations from field sites where the magnitude and timing of base level change can be constrained independently, and where field data sets can be used to reconstruct both fluvial erosivity and

bedrock strength. Rivers crossing active normal faults provide a unique opportunity to constrain both of these parameters simultaneously, as long as slip rates and temporal evolution of faulting are known independently. In this paper we tackle this challenge by collecting a dataset of rock strength and channel geometries to calculate stream power values in a geologically well-constrained catchment responding to active faulting in the Corinth Rift, Greece.

1.1 Calibrating bedrock erodibility

The long term rate of erosion *(E*, in my^{-1}) in bedrock rivers over timescales of 10^4-10^6 years is commonly modelled to be dependent on the specific stream power, ω, scaled by bedrock erodibility k (Tucker and Whipple, 2002; Whipple and Tucker, 2002; Attal et al., 2008; Whittaker et al., 2008). This can be expressed as

$$E = k\omega = k\frac{\rho g Q S}{W_b} \quad \text{(Eq. 1)}$$

where ρ is the density of water, g is the acceleration due to gravity, Q is discharge (m^3s^{-1}), S is local channel slope (y/x) and W_b the local channel width (m). Consequently, it follows that stream power represents energy dissipation per unit channel area of the bed with units of Wm^{-2} (Lavé and Avouac, 2001; Stark, 2006; Whittaker et al., 2007a; Attal et al., 2008; Mudd et al., 2014). Stream power erosion 'laws' are widely implemented in landscape evolution models (Seidl and Dietrich, 1992; Howard et al., 1994; Tucker et al., 2001; Mudd et al., 2014) and in field studies over longer timescales where the details of individual flow events are evidently not knowable over million year periods (Stock and Montgomery, 1999; Kirby and Whipple, 2001; Snyder et al., 2003; DiBiase et al., 2010). Empirical studies of the hydraulic geometry and incision history of bedrock rivers, which have reached topographic steady-state but which cross active normal faults, have shown that the distribution of specific stream power ω balances the distribution of fault-driven footwall uplift (e.g. Whittaker et al., 2007b) suggesting that ω is an appropriate measure as long as hydraulic geometry including channel width is explicitly measured (cf. Whittaker et al., 2007a; Cowie et al., 2008). River long profiles have also been widely used as a tool for deriving spatial and temporal changes in rock uplift rate, (Kirby and Whipple, 2001; Snyder et al., 2003; Wobus et al., 2006; Brocklehurst, 2010; DiBiase et al., 2010; Kirby and Whipple, 2012), although extracting quantitative constraints about tectonics in this way is dependent on a well-constrained value for bedrock erodibility k. However, while most variables and parameters in the stream power equation can be derived from field and DEM data, k cannot be measured directly from rock strength data (Bursztyn et al., 2015). Deriving it from landscapes therefore requires constraints on the geological timing of river evolution. Moreover,

as k is an erodibility coefficient, its value and associated units are explicitly dependent on the precise choice of erosion law (Stock and Montgomery, 1999; Kirby and Whipple, 2001). For bedrock rivers whose erosional dynamics approximate a unit stream power law, k can in principle be constrained in cases where both incision rates and the down-system distribution of stream power can be computed (Stock and Montgomery, 1999; Attal et al., 2008). Such well-constrained field sites are not common.

Nonetheless, there have been studies which have estimated k from topography or from attempting to produce model landscapes that resemble nature. One starting point is Stock and Montgomery (1999), who calibrated stream power equations by forward-modelling river palaeo-profiles, constrained by river terraces and basaltic layers, to presently observed profiles for a range of locations worldwide. They estimated a range of erodibility values varying by five orders of magnitude (10^{-7} to 10^{-2} $m^{0.2}yr^{-1}$) for a drainage-area (rather than discharge) dependent version of the stream power model where the exponent on the slope term $m = 0.4$. Using the same approach, Whipple et al. (2000) obtained erodibilities for a river in Alaska forming a new bedrock channel after a 1912 volcanic eruption, and Kirby and Whipple (2001) quantified the effect of uplift rates on erodibility using measurements from the Siwalik Hills of central Nepal. Both studies reported bedrock erodibilities on the order of 10^{-4} $m^{0.2}yr^{-1}$. Similarly Attal et al. (2008) calibrated a stream power model to a field site in Italy constrained by Whittaker et al. (2007b) and obtained values on the order of 10^{-6} $m^{-1/2}$ s^2 $kg^{-3/2}$ for a shear-stress-dependent formulation of this model. Pechlivanidou et al. (2019) also calibrated erodibility values by comparing modelled and estimated sediment volumes from seismic reflection data, giving erodibility values in the order of 1.5 – 4 x 10^{-6} m^{1-2m} yr^{-1} in the Corinth Rift. None of these field studies compared their findings with independent measures of rock mass strength. Numerical models of landscape evolution have used k values that can produce realistic-looking landscapes, but these are not usually constrained by physical measurements of rock strength: For instance, Roy et al. (2015) modelled more than two orders of magnitude variation in erodibility (3.6 x 10^{-5} to 2 x 10^{-3} m s^2 kg^{-1}), based on the assertion that k can be related to the inverse square of rock cohesion. Yanites et al. (2017) use a similar range of magnitudes, although smaller absolute values to model lithological controls on erosion motivated by the Eastern Jura Mountains of Switzerland. Overall these studies illustrate the paucity of well-calibrated studies of rivers responding transiently to external perturbation where (i) tectonic boundary conditions; (ii) hydraulic geometry and stream power; and (iii) variations in rock mass strength are all simultaneously constrained, enabling estimates of k from (i) and (ii) to be compared with lithologic constraints (iii).

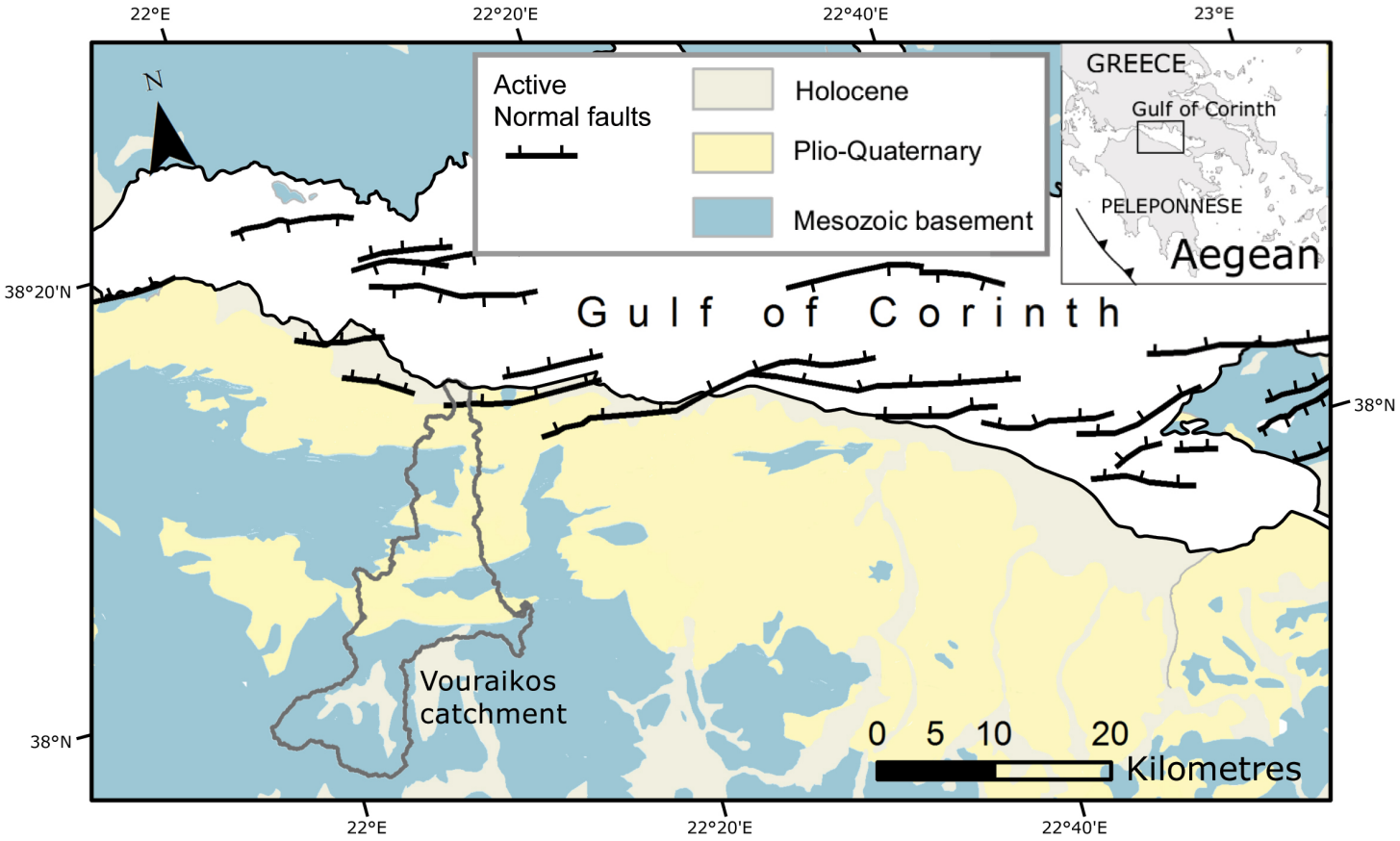

Figure 1 Corinth Rift regional tectonic map with offshore active faults after Nixon et al. (2016) and lithology after Ghisetti and Vezzani (2005), Rohais et al. (2007) and Ford et al. (2013). Holocene and Plio-Quaternary deposits are unconsolidated and consolidated syn-rift delta conglomerates respectively, whilst the Mesozoic basement consists of limestone and flysch (see Fig. 2).

Here, we collect field data in the Corinth rift, central Greece, that allows us to constrain hydraulic geometries, stream power and measurements of bedrock strength for a catchment crossing a well-documented active fault where tectonically driven uplift rates and fluvial incision are known. We use our hydraulic measurements to derive erodibility parameters within a stream power model, and we explore the dependency of these estimates on physical measures of lithological strength. The lithologies range from weak conglomerate to hard limestone bedrock. Importantly, the timing and magnitude of active faulting and river erosion in the last one million years are very well-understood (McNeill et al., 2005; Ford et al., 2013).

The Gulf of Corinth in central Greece is orientated E-W to NW-SE and is ~120 km long and ~30 km at its widest. With modern spreading rates of 5-15 mm yr^{-1}, the Corinth Rift is one of the most rapidly extending rifts in the world (Le Pichon et al., 1995; Briole et al., 2000). Currently the southern margin of the Corinth Rift consists of an array of active north-dipping normal faults (Fig. 1), the oldest of which are known to have activated in the

mid-Pleistocene based on synsedimentary delta deposits and seismic sections (Kontopoulos and Doutsos, 1985; Frydas, 1987; 1989; Ori, 1989; Leeder et al., 2008; Ford et al., 2016).

2 Study location

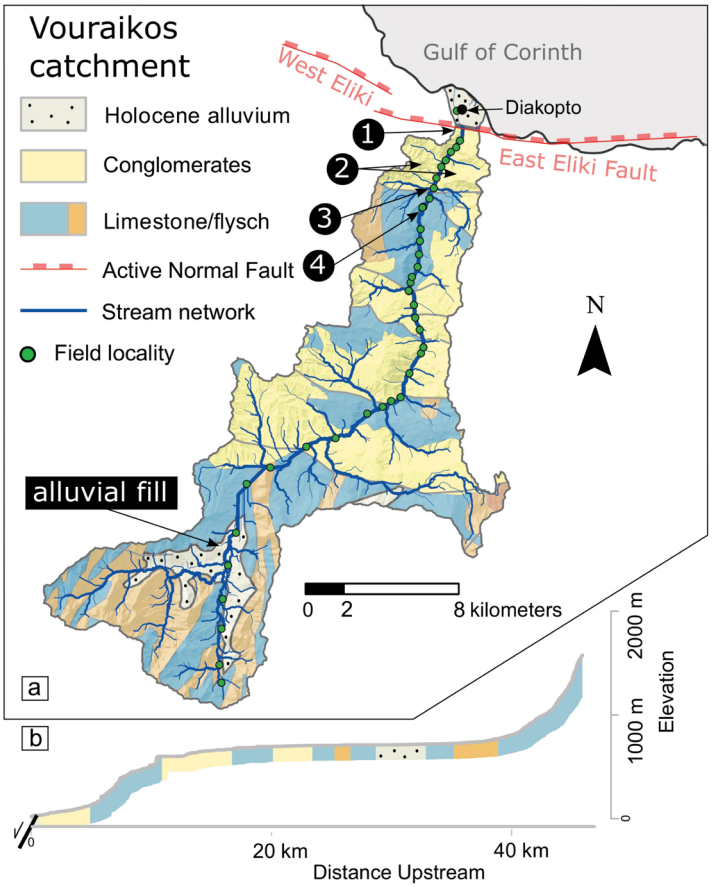

Figure 2 a) The Eliki Fault, Vouraikos catchment, bedrock lithologies, field localities and locations 1-4 of uplift constraints along the river profile (Table 2). b) River long profile of the Vouraikos River. The catchment contains a zone of convexity upstream of the East Eliki fault, whilst in the upper reaches alluvial fill aggrades in the valley.

We focus on the Vouraikos River catchment to investigate the control of lithology on knickpoint propagation because it has extensive neotectonic constraints on uplift and variable bedrock lithology throughout. The Vouraikos River consists of a 46 km long trunk stream with a drainage area of 240 km^2 (Fig. 2a). The base level for the catchment is controlled by the active East Eliki Fault, which is a 15 km long on- and offshore, north-dipping normal fault that crosses the Vouraikos River 2 km from its mouth (McNeill and Collier, 2004; McNeill et al., 2005). Pleistocene climate variations resulted in the formation of marine terraces, which were subsequently uplifted in the footwall of the Eliki Fault (McNeill and Collier, 2004), but the effect of glacial-interglacial sea-level variation on the catchment's base level is limited by the presence of the Rion-Antirion Sill, periodically transforming the Gulf of Corinth into a lake during glacial lowstands. Watkins et al. (2018) demonstrate using global circulation models (GCMs) and proxy data that mean annual precipitation rates in the Corinth Rift have

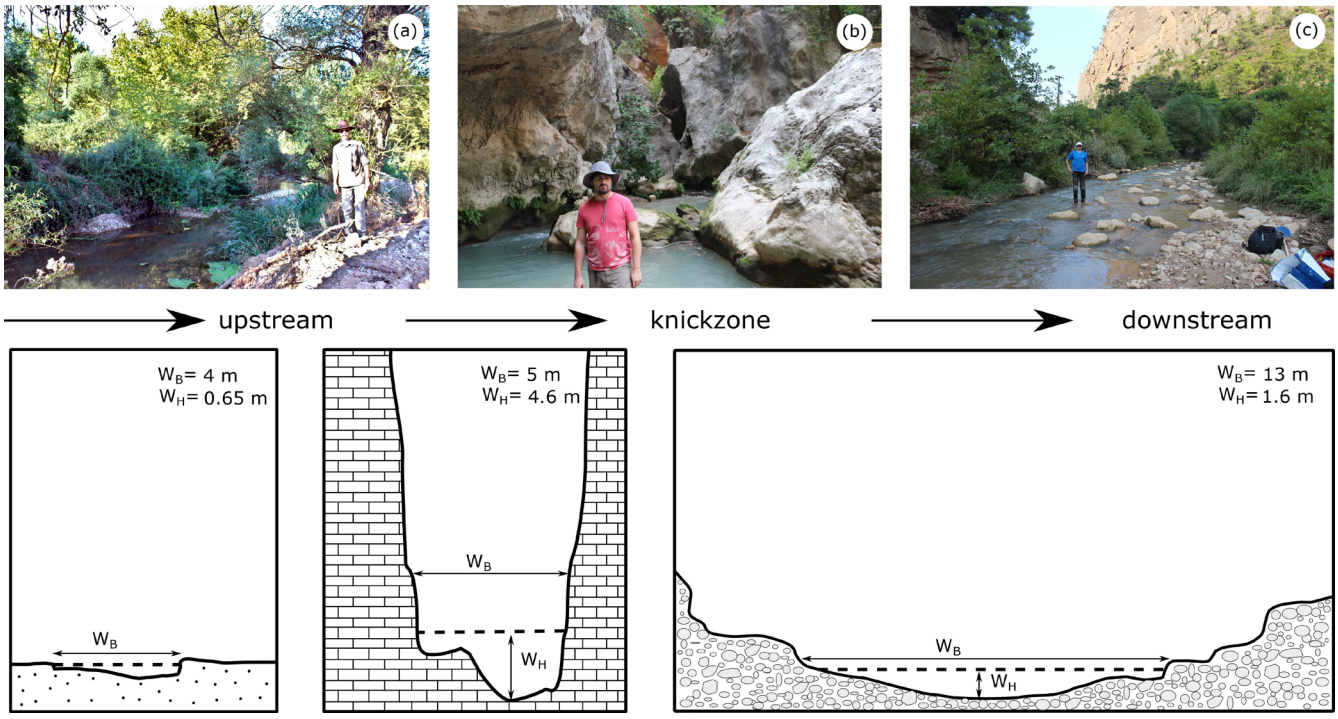

Figure 3 - style of bedrock river throughout the Vouraikos catchment, from a) wide valleys with alluviated channels upstream of the knickpoint, to b) a bedrock gorge and c) a valley incised into conglomerates with coarse alluviated channels near the mouth. Cross sections are reproduced from field observation, with marked on bankfull water level in dashed lines and vertical and horizontal channel lengths given in meters.

not changed significantly over the last glacial-interglacial cycle, with mean annual rainfall averaging at 740 mm yr^{-1}, which is in the range of 716 to 977 mm yr^{-1} predicted by GCMs (Gent et al., 2011; Jungclaus et al., 2013; Sueyoshi et al., 2013) during the Last Glacial Maximum (LGM). Mean annual temperatures in the LGM in GCMs were lower by 5 °C than the modern WorldClim data (Hijmans et al., 2005), with an average of 14.5 °C today and palaeotemperatures between 8.8 and 9.6 °C. Palynology of incised hanging wall Gilbert Delta deposits gives a date of fault initiation at ~0.7 Ma (Ford et al., 2013; Hemelsdaël and Ford, 2016) and footwall uplift rates of 1.00-1.25 mm yr^{-1} are derived from late Pleistocene and Holocene uplifted notches, terraces and beach deposits (Stewart and Vita-Finzi, 1996; De Martini et al., 2004; Pirazzoli et al., 2004). Cross-sections by Ford et al. (2013) report 1600 m of total throw on the fault at its crossing with the Vouraikos River, of which 800 m is footwall uplift. Consequently, the base level change for the Vouraikos has been controlled by the uplift rate of the East Eliki Fault for at least the last 700 ky (McNeill and Collier, 2004).

McNeill and Collier (2004) correlated uplifted marine terraces south of the East Eliki Fault (Fig. 2a label 1) with their compiled sea-level curve, which suggests uplift rates have been approximately constant. Where the Vouraikos River crosses the active fault, however, no fault scarp is present, demonstrating that river incision is keeping pace with fault-driven uplift at this locality (cf. Whittaker et al., 2007b). The Vouraikos catchment

contains at least eleven lithological boundaries between competent limestone and syn-rift sediments as the river flows downstream (Fig. 2b).

A river long profile, taken from a 5 m spatial resolution LiDAR DEM (copyright © 2012, Hellenic Cadastre) shows a very prominent convexity in its long profile, located 7-16 km upstream of the East Eliki Fault (Fig. 2b) which reaches 600 m elevation above the fault. Upstream of this knickzone, our field observations and satellite imagery show that the Vouraikos River is characterised by wide, low relief valleys with more alluviated channels (Fig. 3a), indicating that this part of the river is yet to incise in response to the active fault located downstream. A narrow (10 m) bedrock gorge mostly contains the knickzone (Fig. 3b) and the river widens downstream towards the fault, into a high relief, highly incised valley where the bedrock consists of consolidated early Pleistocene conglomerates through which the river has incised by hundreds of metres (Fig. 3c). The presence of one major knickzone in the Vouraikos catchment, with no sign of other knickpoints at lithological boundaries suggests that lithological boundaries in the Vouraikos catchment alone are not responsible for the shape of the river long profile.

However, significant knickzones upstream of active faults along the south-coast of the Gulf of Corinth are ubiquitous and have been widely interpreted as recording on-going normal faulting in this area (e.g. Demoulin et al., 2015; Fernández-Blanco et al., 2019). Consistent with previous studies, we interpret the presence of the large knickzone in the Vouraikos River (Fig. 2b) to represent a transient response of the river to active normal faulting, specifically to the activation of the East Eliki fault at 0.7 Ma. We note that the tectonic and geomorphic observations above support this interpretation (cf. Whittaker et al., 2007b). Contacts between the limestone and conglomerate bedrock types are generally bounded by inactive high angle faults (Ford et al., 2013) with strata dipping steeply in the deformed limestone basement. Limestone strata are massive beds often exceeding 1 m in thickness without significant fracturing and the conglomerates are similarly structurally homogeneous. Consequently structural discontinuities on the scale that might affect river erosion (e.g. through plucking) are not widespread, or else do not vary significantly within any lithological unit, and the absence of major horizontal boundaries between rocks of differing strength means no complex river erosion dynamics are expected to be driven by lithological control (Forte et al., 2016). Lithology and its range of rock mass strengths may still be expected, however, to have a significant impact on channel geometry and the rates of knickzone propagation upstream generated by the large footwall uplift signal from the active fault. In this paper we combine field data on river geomorphology and synthesise constraints on uplift and incision in the Vouraikos catchment to derive

erodibility values along the river. Further, we compare these to rock strength measurements to constrain the effect of rock strength on erodibility and geomorphological expression of fluvial metrics and knickzones.

Table 1 – Summary of Gulf of Corinth South Coast parameters and uplift rates

Labels corresponding to Fig. 5	Fault	Time average	Slip rate (mm yr^{-1})	Citation	Dip angle	Neo-tectonic indicator	Uplift rate (mm yr^{-1})	Citation
1	West Eliki	Quaternary				Uplifted terraces	1.25	De Martini et al. (2004)
2	East Eliki	Holocene	2.5 - 4.5	McNeill et al. (2005)	50[1]	Palaeoseismic trenching	~ 0.6 to 1.6	This Study
3	East Eliki	Holocene				Uplifted notches	0.9 – 1.5	Stewart and Vita-Finzi (1996)
4	East Eliki	Holocene				Uplifted beach and fauna	1.4 – 2.0	McNeill and Collier (2004)
5	East Eliki	Holocene				Uplifted notches	0.8 – 2.1	Pirazzoli et al. (2004), Stewart and Vita-Finzi (1996)
6	East Eliki	Quaternary				Uplifted terraces	1.0 – 1.2	McNeill and Collier (2004), De Martini et al. (2004)
7	East Eliki	Holocene				Uplifted notches	1.3 – 2.2	Stewart and Vita-Finzi (1996)

[1]scarp field measurements in western edge of East Eliki fault (McNeill et al., 2005) [2] focal mechanisms (Stefatos et al., 2002)

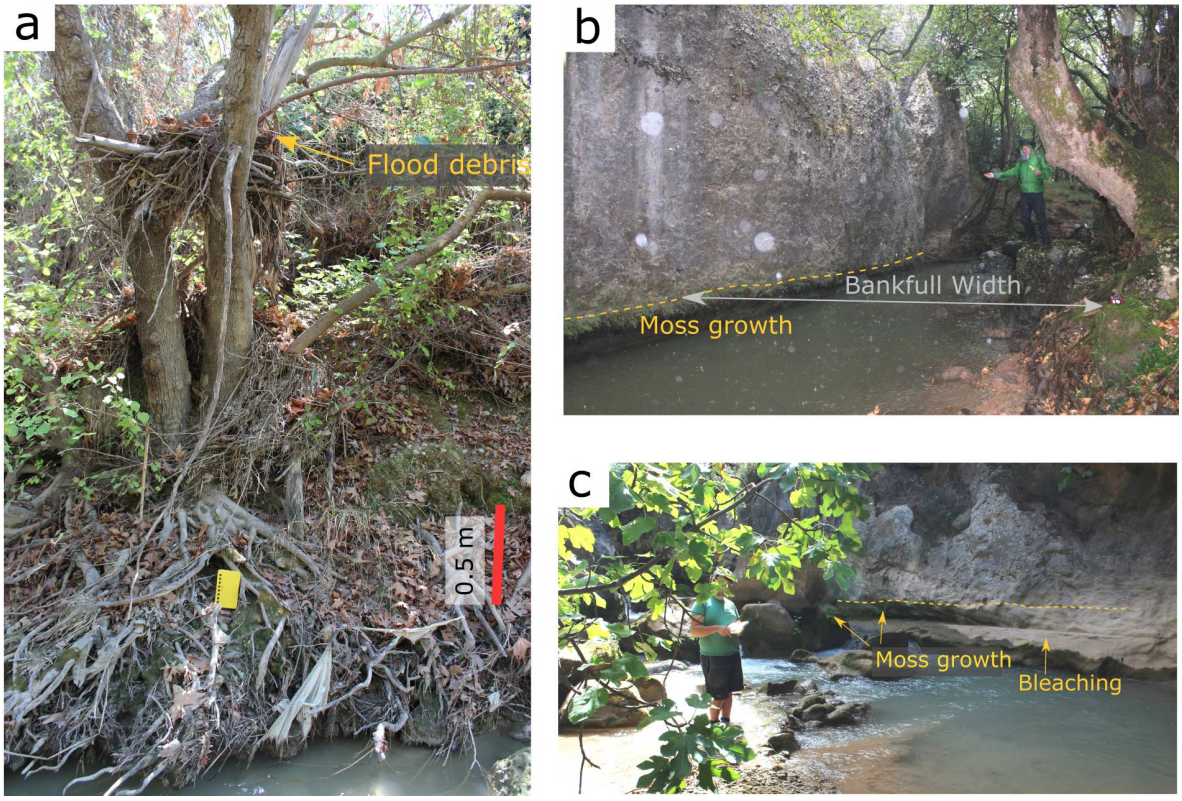

Figure 4 – Photos showing pointers with which bankfull width is estimated in the field, with bankfull height shown as an orange dotted line where appropriate. (a) Flood debris remains in tree branches, (b & c) moss growth and bleaching on boulders and bedrock.

3 Methods

We measured hydraulic geometry to constrain the distribution of stream power down system in the Vouraikos River to calculate bedrock erodibility *k* down-system, using constraints on uplift and incision rates from terraces spanning the last 0.7 Myr. Since Watkins et al. (2018) demonstrated modern precipitation rates are broadly similar to the Last Glacial Maximum, glacial-interglacial climate variation within the last few hundred thousand years won't significantly affect our calculation of *k*. Combined with systematic measurements of rock strength, using a Schmidt hammer as a tool to measure bedrock strength in a field setting, we therefore estimate erodibilities for the limestone and conglomerate bedrock exposed along the river channel and link these to measures of intact rock strength.

3.1 Determination of incision rates in the Vouraikos River catchment

Calculation of the erodibility parameter along the length of the Vouraikos River requires constraints on river channel incision rates and stream power. To derive incision rates along the length of the Vouraikos River, we synthesize uplift constraints along the length of the East Eliki fault, which runs close to where the Vouraikos

River mouth enters the Gulf of Corinth (Fig. 2). We use the resulting uplift rates to model an uplift field offshore along the length of the Vouraikos River, decaying according to a visco-elastic model. Comparison of this field and incision rate constraints present at points along the Vouraikos River enables the verification of the model uplift field as an input for long-term river channel incision rates.

3.1.1 Rates of uplift along the East Eliki Fault

To address the response of the Vouraikos River to active faulting, we need to synthesise existing constraints on neotectonic rates of faulting, which have led to fluvial incision upstream of the East Eliki Fault. Numerous estimates of surface uplift along the East Eliki Fault have been compiled from the literature and are listed in Table 1. These comprise time-averaged Holocene and Quaternary uplift rates from well-known uplifted markers. Time-averaged uplift rates come from palaeo beach remnants such as beach deposits (McNeill and Collier, 2004), wave-cut notches (Stewart and Vita-Finzi, 1996; Pirazzoli et al., 2004) and Quaternary marine terraces (De Martini et al., 2004; McNeill and Collier, 2004). Trench data (McNeill et al., 2005), while showing individual slip events rather than time-averaged uplift, give an indication of minimum slip rates in the last thousand years. Such slip rates were converted into footwall uplift rates using an average fault dip angle of 50° derived from field measurements of the scarp at the western end of the East Eliki fault (McNeill et al., 2005). We use an uplift to subsidence ratio of 1:1.2 to1:2.2 determined by McNeill et al. (2005) by comparing long-term uplifted footwall elevation and hanging wall subsidence from depth-to-basement measurements in seismic reflection data near the East Eliki Fault.

3.1.2 Uplift field across the catchment

Footwall uplift of normal faults is caused by elastic rebound triggered by stress reduction across the fault during slip; the magnitude of uplift decays away from the fault (Bosworth, 1985; Buck, 1988). To constrain the uplift field upstream of the East Eliki Fault, we use the constraints on uplift rates summarised in Table 1 and propagate the uplift field upstream of the Vouraikos River away from the fault using a visco-elastic model calibrated for the Corinth Rift and published by Bell et al. (2017). We use Bell et al.'s (2017) model 2a (see the supplementary material of this paper, Fig. S1), which involves a planar fault dipping at 45° from the surface down to 10 km depth. Bell et al. (2017) found that this model best matches the geological observations of vertical deformation as well as uplift to subsidence ratios determined from seismic profiles across modern faults in the Corinth Rift. We model uncertainty by using the range of uplift estimates at the East Eliki Fault to set a maximum and minimum uplift field for the Vouraikos catchment.

3.1.3 Incision rate constraints

As the East Eliki fault does not exhibit a scarp in the Vouraikos River channel in the field, although its trace is present along strike, we deduce that incision equals uplift where the river crosses the fault (cf. McNeill and Collier, 2004). We further plot markers of river incision upstream against our model for uplift distribution. River incision after the initiation of the East Eliki Fault at 0.7 Ma (Ford et al., 2013) is quantified from the vertical distance between modern river channel elevations and abandoned surfaces (Table 2), such as the marine terraces at the mouth of the Vouraikos River (McNeill and Collier, 2004) and delta top surfaces which extend further inland (Ford et al., 2013). Marine terrace heights (Fig. 2 label 1) and historical sea level are compared (McNeill and Collier, 2004) so that formation altitudes and the height to the modern river can be used to calculate river incision rates (Table 2). The modern river flows over the top of the modern delta, and so we use the elevation of the uplifted delta top surface south of the fault (Fig. 2 label 2) and compare it to modern river elevations. Together with biostratigraphic dates from Ford et al. (2013), which date the top layer of the palaeo-delta and the start of uplift associated with the East Eliki fault at 0.7 Ma, we use these elevations to calculate river incision rates upstream (Table 2).

We make further estimates of minimum incision rates from three fluvial erosional strath terraces. First, two prominent strath surfaces are present at the top of the limestone gorge (Fig. 2 label 4) hosting the knickzone. These mark the onset of incision related to the uplift associated with the East Eliki fault, though it is likely that they got abandoned relatively soon after the imposed uplift field (Maddy, 1997). Just downstream of the bedrock gorge an erosional strath terrace topped with unconsolidated gravels lies just 8 m above the modern river channel. Watkins et al. (2018) note the presence of undated river-fill terraces attributed to the late Pleistocene. Their sediment volume estimations from seismic surveys show an increase in sediment accumulation rates in the Gulf of Corinth from the last glacial to the Holocene, which they attribute to Holocene incision of sediment that accumulated in the catchments during the last glacial Furthermore, the lowest river terraces in Greece, Bulgaria and Turkey typically lie between 5 and 12 m above the modern river and dating of volcanic layers and numerical modelling have linked those the end of the late Pleistocene cold-climate stage MIS 2 (Westaway et al., 2006; Zagorchev, 2007), in keeping with climate-forced fluvial sequences worldwide (Bridgland et al., 2007). Consequently, we assign abandonment of this lower terrace to the end of stage MIS 2 (~12 ka), which would imply an incision rate of ca. 0.7 mm yr^{-1} since this time (Table 2). Ages of abandonment of palaeosurfaces and measured heights above the modern river channel are summarised in Table 2 together with the resultant incision rates.

3.2 Collection of river hydraulic geometry

We made detailed measurements in the field at 500-1000 m intervals upstream (Fig. 2a), totalling more than 30 field locations within the Vouraikos gorge, to constrain: bankfull channel widths (W_b), channel depths (H), and local channel slope (S). We used the 5 m spatial resolution LiDAR DEM (copyright © 2012, Hellenic Cadastre) to calculate drainage area as well as channel slopes which we use to calibrate and quality check against our field measurements of channel slope. We use these data to estimate specific stream power in the channel (Eq. 1). The location of bankfull widths and depths are estimated in the field following the methodologies of previous workers (Montgomery and Gran, 2001; Snyder et al., 2003; Whittaker et al., 2007b) by recording the channel cross-sectional form, and high stage flow markers including the limits of bleaching on bedrock and the remains of flood debris (Fig. 4). We estimate bankfull discharge using Manning's Equation (Manning, 1891):

$$Q = vA = \frac{1}{n}R^{2/3}S^{1/2} * A \quad \text{(Eq. 2)}$$

where v is velocity in m s^{-1}, A is cross sectional area (m^2), R is the hydraulic radius (m) which is the ratio of the cross-sectional area to the wetted perimeter, S is the local channel slope (x/y) and n is Manning's n value which for steep headwater streams is ~ 0.3 (Manning, 1891). We derived representative discharge estimates for repeat sections in the downstream portion of the channel, and scaled these to the drainage area A of the catchment derived from the DEM, making the reasonable assumption that A is proportional to Q so that discharge increases downstream. Subsequently, we derive unit stream power (ω) using equation 1 at every locality measured along the river (Fig. 2a). We explicitly compared the magnitude and distribution of stream power downstream with our reconstruction of footwall uplift rates (cf. Whittaker et al., 2007b) and our estimates of fluvial incision rates to establish where the river has reached an erosional steady state where footwall uplift and fluvial incision rates are similar. Dividing incision rates by stream power values therefore gives us a value for k (Eq. 1) along the incising bedrock reach of the river. We compare the substrate lithology and the values of erodibility downstream to explore the effect of lithology on k. Errors on our erodibility values reflect the uncertainty in channel geometry measurements which propagate into the errors for stream power values.

3.3 Rock strength measurements

A comparison of physically-based rock strength measurements with our derived erodibility values should provide insight into how rock strength influences landscape evolution, given that bedrock erodibility k cannot be measured directly. Numerous methods of measuring intact rock strength, compressive or tensile, exist (Goudie, 2016), and there is considerable debate about which approach 'captures' rock resistance to fluvial erosion most

appropriately (Selby, 1980; Atkinson, 1993; Sklar and Dietrich, 2001; Cai et al., 2004; Brook and Hutchinson, 2008; Jansen et al., 2010; Bursztyn et al., 2015; Roy et al., 2015; Goudie, 2016). For instance, some authors advocate laboratory tensile strength measurements as being the most useful to quantify bedrock erodibility (Sklar and Dietrich, 2001; Bursztyn et al., 2015), while others link erodibility to bedrock cohesion (e.g. Roy et al., 2015). However these measurements cannot easily be made in situ and require sample collection. A semi-quantitative 'Selby' index of bedrock strength, including the distribution and size of jointing and the 'degree' of weathering (Selby, 1980) has also been used in a number of studies, although this approach was not originally intended to quantify bedrock resistance to fluvial erosion and its application to rivers has proven equivocal (Whittaker and Boulton, 2012; Bursztyn et al., 2015). Consequently, we use a Schmidt hammer as a simple and repeatable means to quantify bedrock strength in the field. We do this because it is a portable, convenient and practical way to estimate the uniaxial compressive strength of bedrock in an isolated field setting and it can capture in-situ natural variability (Goudie, 2006; Niedzielski et al., 2009; Viles et al., 2011). Where exposed bedrock was present in the river (shown in Fig. 2a), we made at least twenty rebound measurements at each location, recording Schmidt hammer orientation (horizontal, vertical, angle), totalling more than 360 readings. Where possible we recorded values above and below the waterline, and in those locations we have more than forty readings. Schmidt readings were corrected for hammer orientation to the rock surface to horizontal equivalent readings using the conversion scale on the hammer. In addition, using formulas derived by Yagiz (2009) (see the supplementary material of this paper, equation S2) for a range of carbonate lithologies, we convert Schmidt hammer values to first order estimates of uniaxial compressive strength (UCS).

3.4 Simulation of knickzone propagation

To test whether our k values are broadly reasonable, we use the derived erodibility values to estimate the plan view location of the knickzone 0.7 Ma after fault initiation compared to the observed location. We can do this since theoretical considerations and empirical data sets argue that the vertical and plan view knickpoint propagation vectors are independent (Tucker and Whipple, 2002; Whipple and Tucker, 2002; Wobus et al., 2006; Whittaker et al., 2008; Whittaker and Boulton, 2012). As knickpoint propagation rates control fluvial response times to tectonics (e.g. Whittaker and Boulton, 2012), we also evaluate the timescales of knickpoint retreat if our study catchment were solely composed of either limestone or conglomerate bedrock. For any general form of the stream power erosion law, the horizontal wave celerity C_E of the kinematic wave associated with the propagation of a knickpoint upstream is dependent on the upstream distribution of catchment drainage area A, and is given by

$$C_E \sim \Psi A^m S^{n-1} \quad \text{(Eq. 3)}$$

where coefficient Ψ represents a range of factors, including but not limited to bedrock erodibility (Wobus et al., 2006; Whittaker and Boulton, 2012). For a unit stream power model, n = 1, we can express Ψ as k Φ, where *k* is the bedrock erodibility from Equation 1. Consequently,

$$C_E = k\,\Phi\,\sqrt{A} \quad \text{(Eq. 4)}$$

where Φ includes the scaling of discharge and channel width with drainage area down-system. We adopt this simple form so we can model a range of scenarios for knickpoint retreat (below) using our DEM-derived catchment data and our field constraints. For the scaling of drainage area and discharge we assume a linear relationship with an effective precipitation term (1 m/yr - (Hellenic National Meteorological Service)) and for the channel width we fit a simple hydraulic scaling law (i.e. $W \sim cA^{0.5}$) (Leopold and Maddock Jr, 1953) to our existing field data as explicit predictions of the evolution of channel width over time within the knickzone are non-trivial to generate. As modern precipitation rates are broadly similar to the Last Glacial Maximum (Watkins et al., 2018), and *k* values where calculated using palaeosurfaces recording uplift and incision over the last 0.7 Myr our calculation of knickpoint retreat integrates Pleistocene climate fluctuations in the modelled incision rate. Further details are contained in the supplementary material.

We vary erodibility through the catchment according to three simple scenarios. In the first, erodibility *k* varies along stream according to the two main rock types observed in the field (Fig. 2), and our reconstructed values of *k* for each of them. Two fictional scenarios test where knickpoints might have migrated in a catchment consisting of only limestone or conglomerate bedrock. For each scenario we assume the knickpoint originated at the fault at 0.7 Ma and that the catchment has the same drainage area configuration as the present day. Our estimates of knickpoint propagation are conservative because in this simple approach we do not account explicitly for channel narrowing within the knickzone that does not obey classical hydraulic scaling (cf. Whittaker et al., 2007a), although we do use field data to constrain the relationship between width and drainage area in the Vouraikos River (Supplementary Information). We define the knickzone location in our calculation based on the end-members predicted by the error on the erodibility values of the conglomerate and limestone bedrock: the start of the knickzone is the location predicted by the maximum value of erodibility and the end location of the knickzone is predicted by the minimum value of erodibility. The observed knickzone is the convex reach defined in Figure 6, while our calculations assume that the knickpoint represents a single point. Nonetheless, we use the degree of

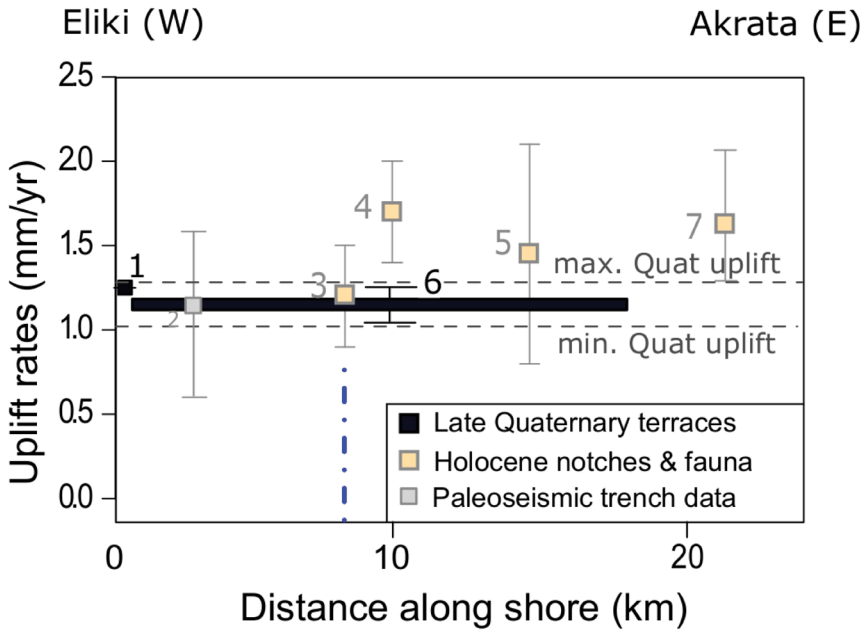

Figure 5 - Uplift rates along the East Eliki Fault (see Fig 2a & Table 1): (black) average Late Quaternary rates (orange) Holocene rates (grey) palaeoseismic trenching. The location of the Vouraikos River is marked as a blue dotted line. The numbered labels match to Table 1. Dashed lines give the maximum and minimum values of Quaternary uplift defined by points 1 and 6.

overlap between the range of knickpoint positions predicted by our calculations, and the location of the real knickzone, to compare our three different scenarios.

4 Results

4.1 Uplift and erosion along the Vouraikos River

Figure 5 provides a synthesis of the evidence and constraints for of uplift rates along the Eliki Fault from Eliki to Akrata from palaeoseismic trenching, Holocene wave-cut notches and uplifted Quaternary marine terraces (Table 1).

Table 2 – Details of erosion rate constraints in the Vouraikos catchment (see section 3.1.3 for methodology, Fig. 6a plots erosion rates against the uplift field)

number on Fig. 2 & 6	Distance upstream (m)	Terrace/surface	Altitude (m)	River altitude (m)	Formation altitude (max scenario) (m)	Formation altitude (min scenario) (m)	min age (kyr)	max age (kyr)	min erosion rate (mm/yr)	max erosion rate (mm/yr)	Citation
Fault scarp (not visible in channels)									1.25	1.25	This study
1	546	marine terraces	110	29	-12	-5	85	115	0.7	1.0	McNeill and Collier (2004)
1	823		195	32	10	-10	130	200	0.8	1.2	
1	928		320	33	-10	-25	210	305	1.0	1.4	
1	1094		365	35	-12	5	240	335	1.0	1.4	
1	1977		550	55	5	-30	335	500	1.0	1.5	
2	1977	palaeo-delta top surface	715	55	19	19	530	800	0.8	1.2	Ford et al. (2007)
2	2110		771	59	29	29	530	800	0.9	1.3	
2	3494		810	81	44	44	530	800	0.9	1.3	
2	3944		820	94	48	48	530	800	0.9	1.3	
3	4140	gorge strath surfaces	118	110	118	118	12	12	0.7	0.7	This study
4	6707		560	460	560	560		700	0.14		
4	10319		580	530	580	580		700	0.1		

Late Quaternary terraces and palaeoseismic trench studies suggest uplift rates on the Eliki fault of 1.00 to 1.25 mm yr^{-1} (Table 1, McNeill et al., 2005; Ford et al., 2007). Similarly Holocene uplift rates reconstructed from published wave-cut notch studies (Stewart and Vita-Finzi, 1996; McNeill and Collier, 2004; Pirazzoli et al., 2004) and palaeoseismic trenching (McNeill et al., 2005) are also within a factor of two of these values (although they are averaged over less time) (Fig. 5). As we are investigating the long term response of the Vouraikos River to faulting since the initiation of the East Eliki fault at 0.7 Ma, we use the Quaternary uplift constraints as the best estimates of longer-term fault uplift rate at the fault and we exploit this evidence to calibrate the visco-elastic fault model outlined in the methods section 3.1.2. We propose three uplift distributions upstream from the East Eliki Fault based on a maximum (1.25 mm yr^{-1}), minimum (1.00 mm yr^{-1}) and average uplift value at the fault derived from Figure 5 (De Martini et al., 2004; McNeill and Collier, 2004) and published by Bell et al. (2017). Uplift starts at the fault and is modelled to decay from 1.00-1.25 mm yr^{-1} (Stewart and Vita-Finzi, 1996; De Martini et al., 2004; Pirazzoli et al., 2004) to zero at 14-15 km upstream, beyond which the catchment experiences relative subsidence in the order of 0.2 mm yr^{-1} based on our model (Fig. 6a).

The relatively-flat valley-fill in the upper reaches of the Vouraikos River Valley (Fig 2a, >30 km upstream of the fault) is also consistent with where we might expect flexure-related relative subsidence to create accommodation space in the distal footwall of the fault. Consequently, the overall pattern in the Vouraikos River is incision upstream of the East Eliki Fault, decreasing and switching to aggradation further upstream as the deformation field changes from uplift to subsidence.

Figure 6a additionally shows how rates of incision from palaeosurface constraints (Table 2) plotted as labelled points vary from 0.8-1.5 mm yr^{-1} at the fault, to a minimum of 0.7 and 0.1 mm yr^{-1} at 8 and 11 km respectively according to maximum ages of terrace abandonment. The match between the modelled uplift-rate field with our erosion rate reconstructions is good (Fig. 6a), and provide good evidence that incision rates decrease upstream of the Vouraikos River in the same way that uplift decays from the proximal to distal footwall of the East Eliki Fault. In the first 7 km upstream of the fault, incision clearly equals uplift. Between 7 and 16 km upstream, in the knickzone, incision equals at least 50% of the reconstructed uplift field and within the uncertainties may account for (almost) all the fault-driven uplift. Consequently, we use our continuous model of the uplift field together with our stream power measurements to calculate erodibility k along stream for two end members (i) E = U within the whole knickzone; or (ii) E = U in the first 7 km upstream of the fault, and E = 0.5U between 7 and 16 km upstream.

4.2 Channel geometry, stream power and erodibility downstream

Figures 6b and c show that channel slopes (y/x) increase from 0.01-0.03 in the Pleistocene conglomerates near the fault to steeper slopes of 0.02-0.18 in the limestone gorge. Upstream of the knickzone, channel gradient decreases and uplift rates become negligible as the lower gradient headwaters of the river are reached. It is also notable that channel widths halve from a range of 9-23 m in the conglomerates near the active fault to values of 4-12 m in the limestone knickzone. These data, derived from more than 30 sets of field measurements, show the Vouraikos River adjusting its hydraulic geometry in response to continued uplift on the East Eliki Fault. The narrowing channels and higher slopes in limestone bedrock are reflected in the stream powers calculated from our field data using Equation 1 (Fig. 6c). Stream powers are very low in the low gradient upper reaches of the river, despite a wide range of mapped bedrock lithology, but reach up to 27 000 Wm^{-2} in the limestone part of the knickzone. This contrasts with values of around 1000 Wm^{-2} further downstream in the 5 km of the river nearest to the active fault, which is where the river cuts through lower Pleistocene conglomerates. This is despite both documented uplift rates and documented incision rates being greater in this reach of the river (Fig. 6a).

We use our constraints on incision rates and our calculations of stream power in the 12 km of the channel upstream of the fault to estimate values of bedrock erodibility, *k* (see equation 1), along this reach of the Vouraikos River. Erodibility decreases upstream from values in the range of 10^{-14} ms^2kg^{-1} in the first 5 km to 10^{-15} ms^2kg^{-1} where conglomerate gives way to limestone bedrock upstream of the fault (Fig. 7). Although *k* values have considerable scatter (Fig. 7), across the lithological boundary the erodibility values jump significantly (Fig. 7). Box and whisker plots (Fig. 7) show the range of values for both conglomerate and limestone for which the mean and standard error values are $1.8 \pm 0.3 \times 10^{-14}$ and $6 \pm 2 \times 10^{-15}$ ms^2kg^{-1} for the scenario where E=U throughout the knickzone. Alternatively we derive a k value for the limestone of $5 \pm 2 \times 10^{-15}$ ms^2kg^{-1} between 7 and 16 km upstream of the fault if we assume that E=0.5U in this region. These data provide evidence for a factor of three to four difference in apparent bedrock erodibility between the upper Pleistocene conglomerates and the limestone. In addition the 360 Schmidt hammer rock strength measurements of the two lithologies we made in the field give rebound values of ~30 (20 MPa UCS) for conglomerate and ~50 (70 MPa UCS) for limestone (Table 3). These results show that a factor of two variation in Schmidt rebound values can translate to a factor of three to four difference in effective bedrock erodibility, *k*.

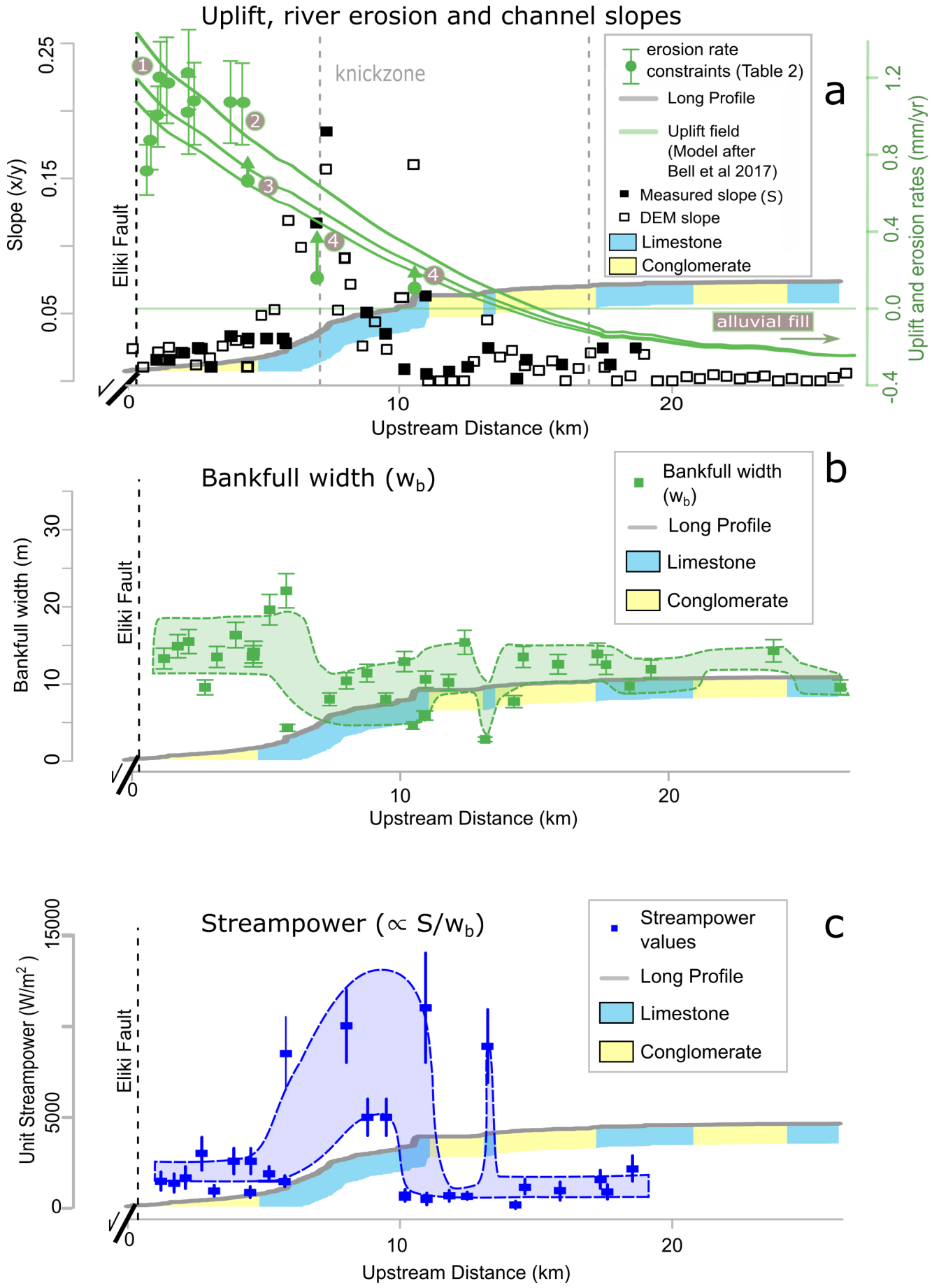

Figure 6 A) river long profile with bedrock lithology (blue = limestone, yellow = conglomerates), uplift along stream with 1-4 independent constraints on erosion rates derived from previously published palaeosurfaces (see Table 2), channel slopes and a knickzone marked by an inversion of the slope gradient. Arrows on erosion rate constraints from abandoned terraces indicate age

constraints are maximum ages of abandonment (see text) B) Bankfull width measured in the field along stream C) Stream power values upstream. Error bars reflect uncertainties in field measurements of channel geometry and discharge.

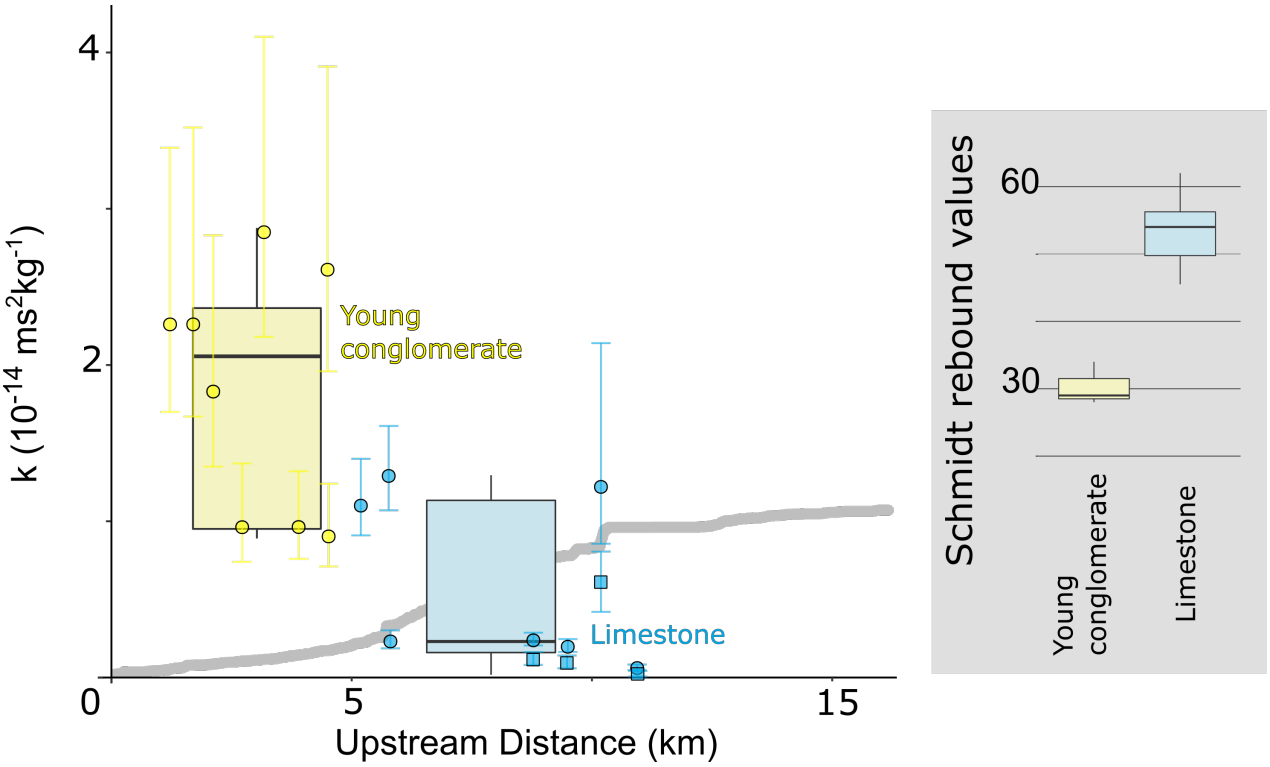

Figure 7 Bedrock erodibility values plotted upstream of the Vouraikos River with profile in grey. Inset shows distribution of >300 Schmidt hammer strength measurements. Error bars reflect uncertainties in field measurements of channel geometry. Square points are from scenario where the erosion rate equals 50% of uplift after 7 km. Box plots show distribution of k values for the two lithologies.

Table 3 - lithological strength measurements converted into uniaxial compressive strength (UCS)

Lithology	Schmidt average (± se)	Schmidt 25th to 75th percentile range	Number of measurements	UCS (MPa)
Conglomerate	29 (± 1)	24 - 32	44	20
Limestone	52.5 (± 0.7)	46 - 61	318	70

4.3 Knickpoint propagation and landscape response times

To what extent is the location of the knickzone in the Vouraikos River consistent with the bedrock erodibility values we have estimated from the analysis of our field data in section 4.2? Figure 8 maps the predictions from our knickpoint calculation upstream, where we use three model scenarios with the same fault initiation date (0.7 Ma) and drainage area of the Vouraikos catchment, but different bedrock erodibilities shown in Figure 7. If the entire catchment were made of conglomerate bedrock with an effective erodibility *k* in the range calculated (Fig. 7), the range of knickpoint locations generated due to the active fault initiating at 0.7 Ma ought to have already propagated into the headwaters of the Vouraikos River to an upstream distance of 32 – 37 km (yellow zone), only 3 km from the catchment divide (Fig. 8). The same scenario with erodibility values deduced for limestone

bedrock would predict the knickpoint to be located between 5 and 20 km upstream (Fig. 8). For a scenario with a distribution of bedrock erodibilities as actually found in the river predicts that the knickpoint should be located at 10 to 29 km. The range of possible knickpoint locations represents the standard deviation on erodibility values used as input for the knickpoint propagation calculation. It is important to note our simple calculations aim to predict the plan view location of the knickpoint following initiation of the East Eliki Fault: we do not seek to forward model the full longitudinal profile evolution of the Vouraikos River over time (Fig. 2). Nevertheless, a match of a range of calculated knickpoint locations and the observed knickzone gives an indication of the validity of our derived *k* values and their standard deviations. The model prediction of the "true" bedrock and the limestone-only scenario match with the location of the knickzone observed today, 7-16 km upstream of the fault (Fig. 6). The initial knickpoint retreat rates for the limestone bedrock in the model is 8 to 28 mm yr^{-1} for a drainage area of 240 km^2 at the fault, whereas for the conglomerate bedrock knickpoint propagation rates start at 60-80 mm yr^{-1}. Both decrease as the knickpoint migrates upstream. These results suggest that our erodibility values derived from vertical erosion constraints do successfully predict horizontal knickpoint migration in our catchment.

The exercise suggests that the lower end of our erodibility estimates are potentially more likely as the upper bound of the predicted range of possible knickpoint locations is more than 10 km beyond the present knickzone (Fig. 8). Moreover, the bedrock geology end-members in terms of erodibility *k* demonstrate the potential response times of catchments to relative base level change, here driven by active faulting, vary on orders of magnitude depending on bedrock lithology. For catchments the size of the Vouraikos River, the model results presented in Figure 8 suggest the change in base level created by the initiation of active faulting to have propagated to the headwaters of the river in ~ 1 Myr if the catchment only contained the weak conglomerate bedrock. In contrast, for a limestone-only catchment, our results show that the signal of base level change due to the fault would take 2.4 to 10 Myr to propagate all the way to the catchment headwaters. Doing the same calculation for the scenario based on the observed mix of lithologies in the Vouraikos catchment gives us a knickpoint propagation time to the end of the catchment of 2.1 to 8.2 Myr. Based on these findings, we suggest that the landscape in the Corinth Rift can record faulting over million year timescales.

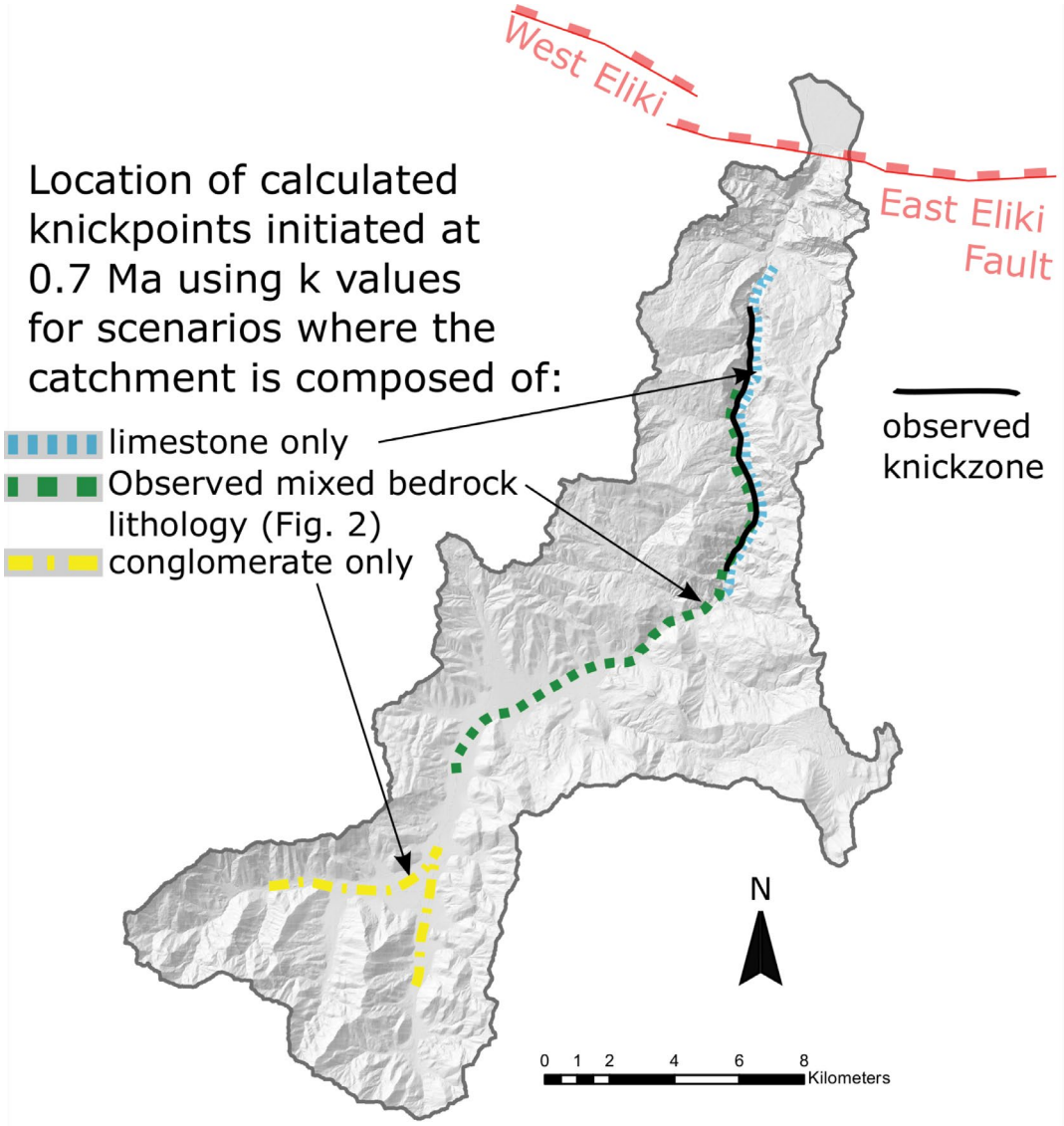

Figure 8 Vouraikos catchment showing zones of predicted knickpoint locations, based on an East Eliki Fault age of onset at 0.7 Ma (Ford et al 2013), for different lithology scenarios. Knickpoint propagation in a conglomerate-only model would have occurred up to the head of the catchment (32-37 km upstream from the East Eliki fault), while a limestone model predicts the knickpoint at 5-20 km, and a mixed lithology model true to the lithological map (Fig 2) predicts a range of possible knickpoint locations 10-29 km upstream from the East Eliki fault. The limestone and 'natural' scenario match the real-world situation (black line) within error.

5 Discussion and implications

Our synthesis of uplift rates on the Eliki Fault (Fig. 5), our visco-elastic model of uplift along the length of the river and our calculation of incision rates from palaeosurfaces dating back to 0.7 Ma (Fig. 6a) provide evidence that incision rates in the Vouraikos River on the southern margin of the Corinth Rift match uplift rates in the footwall of the East Eliki Fault up to the knickzone 7-16 km upstream, where incision rates equal at least half the uplift rates. Our field data show that channel slopes increase and channel widths decrease where the substrate changes from conglomerates to limestones (Fig. 6a-b), increasing stream power by an order of magnitude to counter the change in resistance to erosion (Fig. 6c). The resultant calculated erodibilities differ for conglomerate and limestone bedrock by a factor of three to four (Fig. 7). We thus calculate that the complete propagation of a

knickpoint through the Vouraikos catchment (240 km^2) takes ~1 Ma in conglomerate bedrock and 2.4 – 10 Ma in limestone bedrock. We calculate the response time of 2.1 - 8.2 Ma in the Vouraikos River with the observed lithologies in the catchment (Fig. 2).

5.1 Rock erodibility and its relationship to rock strength

It is important to consider how our constraints on bedrock erodibility compare to those suggested by previous workers. However, studies deriving erodibility values have employed different erosional models or forms of the stream power equation, and therefore units of erodibility vary. Many use the general form of the stream power equation

$$E = KA^m S^n \quad \text{(Eq. 5)}$$

(Whipple and Tucker, 1999), where K is the erodibility parameter, S is channel slopes, m and n are constants, and discharge and channel width are assumed to be a function of drainage area A; these studies often cite their erodibility values in units of m$^{(1-2m)}$ yr^{-1} (e.g. Stock and Montgomery, 1999; Pechlivanidou et al., 2019). Since our study calculates discharge and specific stream power based on extensive field measurements of channel geometry, our derivation of the erodibility values k includes no assumptions on the relation between channel geometry and drainage area. Consequently, our units of erodibility k follow SI units (m s^2 kg^{-1}) and are identical to the inverse of stress.

Comparing our values to most other publications requires conversion from s^{-1} to yr^{-1} and multiplication with constants otherwise subsumed in K calculations. These are the scaling constants of channel width to drainage area (10^{-3}), the constant of gravity (~10 m s^{-2}), precipitation (1 m yr^{-1}) and the density of water (1000 kg m^{-3}) (see supplementary material equation S4) and multiplying these with our values (section 4.2, Fig. 7) gives erodibility values of $0.6 \pm 0.1 \times 10^{-5}$ yr^{-1} and 1.6 - $2 \pm 0.6 \times 10^{-6}$ yr^{-1} for the conglomerates and limestones respectively. Table 4 lists erodibility studies from other studies in comparable units. The inclusion of precipitation in the erodibility values reported in the literature makes comparison tricky when study locations are not in the same climatic zones: the table lists the erodibility values from studies with their Köppen - Geiger climate classification. Nonetheless, erodibility values reported for limestone are on the order of $10^{-7} - 10^{-6}$ m^{1-2m} yr^{-1} (Whittaker and Boulton, 2012; Pechlivanidou et al., 2019) or 10^{-6} m$^{-1/2}$ s^2 kg$^{-3/2}$ (Attal et al., 2008), matching our results. However, to make conclusions based on the range of published erodibility values it important to ask whether

erodibility values are comparable even though choices of stream power law, and thus units, differ slightly between studies (see section 1.1). Even though the choice of parameter values *m* and *n* in the stream power equation leads to a range of units and will influence the magnitude of the values (e.g. Roberts and White, 2010), the match of limestone erodibility values across studies suggests that given a plausible stream power erosion law, the values are affected by less than an order of magnitude by those choices. On the other hand, the range of erodibility values for weak mudstones to strong granites and marbles is much larger, up to five orders of magnitude: from weak mudstones and shales in humid environments (10^{-2} $m^{0.2}/yr$) (Stock and Montgomery, 1999) to granites, metamorphic rock and hard limestones in humid subtropical environments (10^{-7} $m^{0.2}/yr$) (Stock and Montgomery, 1999). This supports the notion that differences in *m* and *n* are not as important as changes in climate or lithology. In addition, contrary to the studies listed above, the comparison of rock strength and rock erodibility for rock types within one catchment enables us to isolate the effect of rock type on erodibility. The calculation of erodibility using the unit stream power law (Eq. 1) further allows us to compare our erodibility values to those of modelling studies using similar stream power laws. We note that recent numerical modelling by Yanites et al. (2017) in the context of the Jura mountains of Switzerland used values of erodibility in identical SI units but 8 orders of magnitude greater: *ca.* 10^{-6} m s^2 kg^{-1} although the rock types they modelled were broadly comparable with those in our study, implying they may have overestimated the erodibility of rock types in their study Similarly Roy et al. (2015) used values as large as 10^{-3} m s^2 kg^{-1} in their theoretical modelling, which implies a landscape vastly more erodible than the real rocks in our study. Our study therefore underlines the importance of field calibration of bedrock erodibility where the timescale and magnitude of landscape responses to e.g. tectonics can be constrained independently.

Table 4 - Erodibility values (k or K) derived or used in studies, their units form of the stream power equation.

Paper	K value	K units	K function	Location	lithologies	Climate
This study	$5 - 6 \times 10^{-15}$ & 1.8×10^{-14}	$m\ s^2\ kg^{-1}$ (Pa^{-1})	$E = k\ pg\frac{Q}{W}S$	Corinth Rift, Greece	Limestone and conglomerate	Mediterranean
	$1.6 - 2 \times 10^{-6}$ & 0.6×10^{-5}	yr^{-1}	$E = KA^{0.5}S^{1.0}$			
Stock and Montgomery (1999)	$10^{-7} - 10^{-6}$	$m^{0.2}/yr$	$E = KA^{0.4}S^{1.0}$	Australia;	Granite and metamorphic	Humid subtropical;
	$10^{-5} - 10^{-4}$			Hawaii, California, Japan	Volcaniclastic	Tropical rainforest, Mediterranean, Humid continental
	$10^{-4} - 10^{-2}$			Japan	mudstone	Humid continental
Whipple et al. (2000)	$2.4 \times 10^{-4} - 9.0 \times 10^{-4}$	$m^{0.2}/yr$	$E = KA^{0.4}S^{1.0}$	Alaska	Sandstone and siltstone	Cool continental
Kirby and Whipple (2001)	$4.3 \pm 0.8 \times 10^{-4}$	$m^{0.2}/yr$	$E = KA^{0.4}S^{1.0}$	Himalaya	Sandstone and conglomerate	Monsoon highland
Attal et al. (2008)	$8.1 \times 10^{-6} - 10.1 \times 10^{-6}$	$m^{-1/2}\ s^2\ kg^{-3/2}$	$E = k_b\tau^{3/2}$	Apennines, Italy	Limestone	Mediterranean
Pechlivanidou et al. (2018)	$1.5 \times 10^{-6} - 2 \times 10^{-6}$	$m^{-1/2}\ s^2\ kg^{-3/2}$	$E = KA^{5/8}S^{19/16}$	Sperchios Rift, Greece	Sandstone and siltstone	Mediterranean
Pechlivanidou et al. (2019)	$4 \times 10^{-6} - 1.5 \times 10^{-6}$	$m^{1-2\,m}/yr$	$E = KA^mS^n$	Corinth Rift, Greece	Conglomerate and limestone	Mediterranean
Whittaker and Boulton (2012)	$1 \times 10^{-7} -> 2 \times 10^{-6}$	yr^{-1}	$C_E = k\ \Phi\ \sqrt{A}$	Turkey and Italy	Limestones, siltstones, sandstones, conglomerates	Mediterranean
Yanites et al. (2017)	$5 \times 10^{-7} - 6 \times 10^{-5}$	$m^{-1/2}\ s^2\ kg^{-3/2}$	$E = k_b\tau^{3/2}$	Modelling study		
Roy et al. (2015)	$10^{-6} - 10^{-3}$	$m\ s^2\ kg^{-1}$ (Pa^{-1})	$E = k\ pg\frac{Q}{W}S$	Modelling study		

5.2 Linking rock strength and bedrock erodibility

Our approach to deriving *k* gives additional insight into the relationship between lithology, rock strength and erodibility. Unlike some previous studies, the presence of a weak and a resistant bedrock type in the same catchment with the same boundary conditions enables direct comparison between lithology and erodibility. In addition, our channel width measurements and discharge calculations enable calculation of erodibility values that exclude climate and channel width scaling parameters. Our results show that the conglomerates in the Vouraikos River are a factor of three to four more erodible than the limestones. Furthermore, Schmidt hammer rebound values are a factor of two apart for the respective lithologies (Fig. 7, Table 3). Thus, for a doubling in Schmidt rebound values from ~30 to >50 (implying compressive strengths of 20 and 70 MPa respectively (Table 4), we see a significant influence on bedrock erodibility values. Such a change in *k* highlights the importance of rock strength variation in interpreting landscapes using stream power models.

Ultimately, a correlation between measurements of rock strength and erodibility would enable the direct translation of known material properties of bedrock into erodibility values for landscape modelling. To derive such a correlation, it is important to consider what the most appropriate measure of rock strength is from both theoretical and practical perspectives. Studies like Bursztyn et al. (2015) and Sklar and Dietrich (2001) correlate tensile rock strength with stream power and erosion respectively. Bursztyn et al. (2015) found a power law relation between tensile strength of the bedrock and stream power, whilst Sklar and Dietrich (2001) found an inverse square relationship between tensile strength and erosion rate; both imply a non-linear relationship between measures of rock strength and bedrock erodibility. Tensile strength effectively represents the resistance to sediment impacts on the riverbed and its use has been advocated based on the stronger correlation of fluvial metrics with Brazilian tensile tests (BTS) than compressive strength (Bursztyn et al., 2015). However measurements of tensile strength cannot be quickly achieved in the field, while Schmidt hammer rebound readings are widely reported. Moreover, since UCS and BTS strength correlate (UCS ~ 10*BTS; Kahraman et al., 2012) Schmidt rebound values provide practical insight and can be replicated elsewhere. Of course neither approach explicitly includes other factors influencing bedrock erodibility including the degree of weathering and jointing, and we strongly suspect that this contributes to the variation in the results we (and others) report.

Not only is the effect of lithological strength apparent in the range of erodibility values we obtained, the range of rock strengths in the Vouraikos River visibly affects the fluvial geomorphology observed. Figure 6 shows that across the conglomerate-limestone bedrock boundary representing a doubling in Schmidt rebound strength, channel widths half and slopes increase by nearly tenfold. Allen et al. (2013) found an up to tenfold decrease in channel widths for a doubling in Schmidt rebound values in the Siwalik hills in the Himalayas while Bursztyn et al. (2015) finds a linear relationship between mean channel gradient and rock tensile strength and a square root between tensile strength and channel width. Thus, compared to these studies slopes along the Vouraikos River respond significantly to lithology, and at the same time channel widths in the knickzone and further downstream are smaller in the high strength limestone then in the weaker conglomerate substrate (Fig. 6b). We hypothesise that this sensitivity in channel slope may be due to the high uplift rates experienced by rivers draining the southern margin of the Corinth Rift (cf. Whittaker and Boulton, 2012). Crossing downstream into the knickzone, channel slopes in the limestone bedrock increase more than the channel slopes in the conglomerate bedrock (Fig. 6a), meaning the expression of the knickpoint is greatest in limestone bedrock. Hence, lower bedrock erodibility results in higher contrasts in channel slopes of rivers responding to tectonic signals, making knickzones more prominent in erosion-resistant landscapes.

5.3 Assumptions, limitations and future research needs

In our approach we have assumed erosion can be described by a simple stream power erosion model and consequently we do not address issues such as (unknown) changing sediment fluxes through the catchment over glacial-interglacial cycles – i.e. we assume detachment limited erosion dominates. Furthermore, we do not consider the effect of varying discharge in our model as GCMs suggest that precipitation, and thus discharge, did not change much over the last glacial-interglacial cycle (Watkins et al., 2018). Hence our results and model can be used to draw conclusions about the long-term rates of knickpoint migration and the propagation through a river with variable bedrock, but not to draw conclusions on the effect of glacial-interglacial cycles on rates and knickpoint expression. To further enhance models of knickpoint propagation further, the potential effect of sediment bedload supply to the river during glacial and interglacial periods would need to be quantified, together with the consequent effect on river incision rates. However, even if sediment flux variations over the last 700 kyr mean that river channel geometries, and thus unit stream power values, changed over time, the effect on the calculation of bedrock erodibility values would be the same for all lithologies within the river. Furthermore, the

correspondence of our calculated knickpoint locations using our derived *k* values with the observed knickzone (Fig. 8) suggests that our values can be successfully used to reconstruct long-term knickpoint propagation rates.

5.4 Implication for landscape response times

River long profiles are often used in tectonic geomorphology to infer tectonic boundary conditions, such as changes in rates of uplift over Quaternary timescales (e.g. Kirby and Whipple, 2001; Snyder et al., 2003; Bishop et al., 2005; Wobus et al., 2006; Brocklehurst, 2010; DiBiase et al., 2010; Kirby and Whipple, 2012). In some cases, entire uplift histories are inferred based on the inversion of river long profiles (e.g. Roberts and White, 2010). In these cases, timescales of tectonic perturbations can only be guessed by comparison with well-constrained field sites such our Corinth Rift site, or by derivation of an average *K* value across large regions undergoing continental-scale uplift (e.g. Roberts and White, 2010). However, the ability to interpret a tectonic history for a landscape based on the absence or presence of knickpoints depends on the ability to estimate rates of knickpoint propagation. In particular, the effect of the erodibility parameter on the evolution of long-profiles might depend on the spatial scale and geological background against which the interpretation is attempted. Because of the strong control of lithology on bedrock erodibility deduced from our field observations (Fig. 7), our data imply a large difference in fluvial (and landscape) response times to tectonic perturbations when we simulate the retreat of a knickzone generated by the initiation of the East Eliki fault. We calculated that for a catchment consisting solely of weak conglomeratic bedrock, a knickpoint would have propagated to the headwaters of the Vouraikos catchment, more than 45 km upstream, within ~1 Myr. Consequently, limited evidence in the river long profile for the tectonic perturbation at 0.7 Ma would be visible today (Fig. 8). In contrast, the presence of the resistant limestone bedrock slows the migration of the wave of incision due to the initiation of the active fault, meaning that the knickpoint is prominent in the river long profile and in the landscape generally as a gorge (Fig. 8). Our results imply that when searching for tectonic signals in the landscape, workers should explicitly consider that the strength of bedrock strongly controls the timescale over which such signals disappear. Based on our data, we estimate the landscape response times for the Vouraikos catchment to the initiation of the East Eliki Fault is 2.1 – 8.2 My. Whilst studies working with long profiles and knickpoints on continental scales may elect to use an average erodibility value (e.g. Roberts and White, 2010; Roberts, 2019), it is apparent from our study that on the scale of medium catchments on the order of 200-300 km^2, with lithology varying on the order of 5-10 km, the erodibility of bedrock greatly influences the expression of knickpoints in the landscape. Hence, when using the landscape to investigate the histories and mechanisms of

single faults or fault arrays such as in the Corinth Rift, it is important to consider explicitly the effect of varying bedrock erodibility (cf. Roy et al., 2015; Forte et al., 2016; Yanites et al., 2017; DiBiase et al., 2018).

6. Conclusions

Our results demonstrate that bedrock erodibility can vary significantly where Schmidt hammer measurements of intrinsic rock strength differ by a factor < 2, and show that rock strength plays a major role in mediating the speed at which the signal of active faulting is translated to landscapes. Within the knickzone upstream of the East Eliki fault in the Corinth Rift, a combination of channel geometry data shows an order of magnitude increase in stream power (1 kWm^{-2} to 27 kWm^{-2}) at the lithological boundary between weak conglomerates and resistant limestone bedrock with Schmidt hammer compressive strengths of ca. 30 and 50 respectively. Such a strong increase in stream power in the Vouraikos River is the product of a halving of channel widths and a tenfold increase in river channel slopes, implying that variable rock strength represents an important control on fluvial geomorphology especially in tectonically active areas. Uplift rates decrease from 1.0-1.2 mm/yr at the fault, 2 km upstream from the Vouraikos River mouth, to zero 14-15 km upstream, and a combination of a visco-elastic model of uplift decaying away from the fault and palaeosurfaces dating back to 0.7 Ma show river incision rates match uplift rates up to the knickzone upstream of the fault, where incision rates equal at least half the uplift rates. These constraints provide input for the calculated erodibility values which are $1.8 \pm 0.3 \times 10^{-14}$ and $5 - 6 \pm 2 \times 10^{-15}$ ms^2kg^{-1}, for conglomerate and limestone substrate respectively. This study demonstrates a three to four-fold decrease in erodibility for a two-fold increase in rock strength, and consequently our calculation of propagation of the knickpoint by headward retreat imply that the timescale for the signal of active faulting to propagate upstream into the headwaters is 2.1 - 8.2 Myr. In a similar catchment to the Vouraikos River with a drainage area of 240 km^2 this would be ~1 Myr if the catchment were underlain by conglomeratic lithologies. However, this response timescale would increase to 2.4 - 10 Myr if the catchment were made up of the limestone unit documented here. These results reaffirm that when interpreting tectonic boundary conditions from the river long profile record on scales of single faults and fault arrays, lithological strength of bedrock is a crucial variable. This study has implications for deriving tectonic rates from topography, and provides calibration inputs for numerical models aimed at decoding river long profiles.

Acknowledgements

We would like to thank the Hellenic Cadastre & Mapping Agency S.A for the use of the 5m Digital Elevation Model. Zondervan and Hann acknowledge support from Imperial College London as part of their MSci programme. Bell and Whittaker were supported by Royal Society grant RG140109.

Declarations of interest: none

References

Allen, G.H., Barnes, J.B., Pavelsky, T.M., Kirby, E., 2013. Lithologic and tectonic controls on bedrock channel form at the northwest Himalayan front. Journal of Geophysical Research: Earth Surface, 118(3), 1806-1825. doi:10.1002/jgrf.20113

Atkinson, R.H., 1993. 5 - Hardness Tests for Rock Characterization. In: J.A. Hudson (Ed.), Rock Testing and Site Characterization. Pergamon, Oxford, pp. 105-117. doi:10.1016/B978-0-08-042066-0.50012-4

Attal, M., Tucker, G.E., Whittaker, A.C., Cowie, P.A., Roberts, G.P., 2008. Modeling fluvial incision and transient landscape evolution: Influence of dynamic channel adjustment. Journal of Geophysical Research, 113(F3). doi:10.1029/2007jf000893

Bell, R.E., Duclaux, G., Nixon, C.W., Gawthorpe, R.L., McNeill, L.C., 2017. High-angle, not low-angle, normal faults dominate early rift extension in the Corinth Rift, central Greece. Geology, 46(2), 115-118. doi:10.1130/G39560.1

Berlin, M.M., Anderson, R.S., 2007. Modeling of knickpoint retreat on the Roan Plateau, western Colorado. Journal of Geophysical Research: Earth Surface, 112(F3). doi:10.1029/2006JF000553

Bishop, P., Hoey, T.B., Jansen, J.D., Artza, I.L., 2005. Knickpoint recession rate and catchment area: the case of uplifted rivers in Eastern Scotland. Earth Surface Processes and Landforms, 30(6), 767-778. doi:10.1002/esp.1191

Bosworth, W., 1985. Geometry of Propagating Continental Rifts. Nature, 316(6029), 625-627. doi:10.1038/316625a0

Bridgland, D.R., Keen, D., Westaway, R., 2007. Global correlation of Late Cenozoic fluvial deposits: a synthesis of data from IGCP 449. Quaternary Science Reviews, 26(22-24), 2694-2700. doi:10.1016/j.quascirev.2007.09.006

Briole, P., Rigo, A., Lyon-Caen, H., Ruegg, J.C., Papazissi, K., Mitsakaki, C., Balodimou, A., Veis, G., Hatzfeld, D., Deschamps, A., 2000. Active deformation of the Corinth rift, Greece: Results from repeated Global Positioning System surveys between 1990 and 1995. Journal of Geophysical Research: Solid Earth, 105(B11), 25605-25625. doi:10.1029/2000jb900148

Brocklehurst, S.H., 2010. Tectonics and geomorphology. Progress in Physical Geography, 34(3), 357-383. doi:10.1177/0309133309360632

Brook, M.S., Hutchinson, E., 2008. Application of rock mass classification techniques to weak rock masses: A case study from the Ruahine Range, North Island, New Zealand. Canadian Geotechnical Journal, 45(6), 800-811. doi:10.1139/T08-019

Buck, W.R., 1988. Flexural Rotation of Normal Faults. Tectonics, 7(5), 959-973. doi:10.1029/TC007i005p00959

Bursztyn, N., Pederson, J.L., Tressler, C., Mackley, R.D., Mitchell, K.J., 2015. Rock strength along a fluvial transect of the Colorado Plateau – quantifying a fundamental control on geomorphology. Earth and Planetary Science Letters, 429, 90-100. doi:10.1016/j.epsl.2015.07.042

Cai, M., Kaiser, P.K., Uno, H., Tasaka, Y., Minami, M., 2004. Estimation of rock mass deformation modulus and strength of jointed hard rock masses using the GSI system. International Journal of Rock Mechanics and Mining Sciences, 41(1), 3-19. doi:10.1016/S1365-1609(03)00025-X

Campforts, B., Govers, G., 2015. Keeping the edge: A numerical method that avoids knickpoint smearing when solving the stream power law. Journal of Geophysical Research: Earth Surface, 120(7), 1189-1205. doi:10.1002/2014jf003376

Chittenden, H., Delunel, R., Schlunegger, F., Akçar, N., Kubik, P., 2014. The influence of bedrock orientation on the landscape evolution, surface morphology and denudation (10Be) at the Niesen, Switzerland. Earth Surface Processes and Landforms, 39(9), 1153-1166. doi:10.1002/esp.3511

Cook, K.L., Whipple, K.X., Heimsath, A.M., Hanks, T.C., 2009. Rapid incision of the Colorado River in Glen Canyon – insights from channel profiles, local incision rates, and modeling of lithologic controls. Earth Surface Processes and Landforms, 34(7), 994-1010. doi:10.1002/esp.1790

Cowie, P.A., Whittaker, A.C., Attal, M., Roberts, G., Tucker, G.E., Ganas, A., 2008. New constraints on sediment-flux–dependent river incision: Implications for extracting tectonic signals from river profiles. Geology, 36(7), 535. doi:10.1130/g24681a.1

Crosby, B.T., Whipple, K.X., 2006. Knickpoint initiation and distribution within fluvial networks: 236 waterfalls in the Waipaoa River, North Island, New Zealand. Geomorphology, 82(1-2), 16-38. doi:10.1016/j.geomorph.2005.08.023

De Martini, P.M., Pantosti, D., Palyvos, N., Lemeille, F., McNeill, L., Collier, R., 2004. Slip rates of the Aigion and Eliki Faults from uplifted marine terraces, Corinth Gulf, Greece. Comptes Rendus Geoscience, 336(4–5), 325-334. doi:10.1016/j.crte.2003.12.006

Demoulin, A., Beckers, A., Hubert-Ferrari, A., 2015. Patterns of Quaternary uplift of the Corinth rift southern border (N Peloponnese, Greece) revealed by fluvial landscape morphometry. Geomorphology, 246, 188-204. doi:10.1016/j.geomorph.2015.05.032

DiBiase, R.A., Denn, A.R., Bierman, P.R., Kirby, E., West, N., Hidy, A.J., 2018. Stratigraphic control of landscape response to base-level fall, Young Womans Creek, Pennsylvania, USA. Earth and Planetary Science Letters, 504, 163-173. doi:10.1016/j.epsl.2018.10.005

DiBiase, R.A., Whipple, K.X., Heimsath, A.M., Ouimet, W.B., 2010. Landscape form and millennial erosion rates in the San Gabriel Mountains, CA. Earth and Planetary Science Letters, 289(1), 134-144. doi:10.1016/j.epsl.2009.10.036

Fernández-Blanco, D., de Gelder, G., Gallen, S., Lacassin, R., Armijo, R., 2019. Transient rivers characterize evolving crustal-scale flexure in the Corinth Rift. EarthArXiv. doi:10.31223/osf.io/8w7kf

Ford, M., Hemelsdaël, R., Mancini, M., Palyvos, N., 2016. Rift migration and lateral propagation: evolution of normal faults and sediment-routing systems of the western Corinth rift (Greece). Geological Society, London, Special Publications, SP439.415. doi:10.1144/sp439.15

Ford, M., Rohais, S., Williams, E.A., Bourlange, S., Jousselin, D., Backert, N., Malartre, F., 2013. Tectono-sedimentary evolution of the western Corinth rift (Central Greece). Basin Research, 25(1), 3-25. doi:10.1111/j.1365-2117.2012.00550.x

Ford, M., Williams, E.A., Malartre, F., Popescu, S.M., Nichols, G., 2007. Stratigraphic architecture, sedimentology and structure of the Vouraikos Gilbert-type fan delta, Gulf of Corinth, Greece. In: G. Jarvis, E. Nichols, C. Paolo (Eds.), Sedimentary processes, environments and basins: a tribute to Peter Friend, pp. 49-90. doi:10.1002/9781444304411.ch4

Forte, A.M., Yanites, B.J., Whipple, K.X., 2016. Complexities of landscape evolution during incision through layered stratigraphy with contrasts in rock strength. Earth Surface Processes and Landforms, 41(12), 1736-1757. doi:10.1002/esp.3947

Frydas, D., 1987. Kalkiges Nannoplankton aus dem Neogen von NW-Peloponnes. Neues Jahrbuch fur Geologie und Palaontologie Monatshefte, 5, 274-286.

Frydas, D., 1989. Biostratigraphische Untersuchungen aus dem Neogen der NW-und W-Peloponnes, Griechenland. Neues Jahrbuch fur Geologie und Palaontologie Monatshefte, 6, 321-344.

Gent, P.R., Danabasoglu, G., Donner, L.J., Holland, M.M., Hunke, E.C., Jayne, S.R., Lawrence, D.M., Neale, R.B., Rasch, P.J., Vertenstein, M., Worley, P.H., Yang, Z.-L., Zhang, M., 2011. The Community Climate System Model Version 4. Journal of Climate, 24(19), 4973-4991. doi:10.1175/2011jcli4083.1

Ghisetti, F., Vezzani, L., 2005. Inherited structural controls on normal fault architecture in the Gulf of Corinth (Greece). Tectonics, 24(4). doi:10.1029/2004tc001696

Goudie, A.S., 2006. The Schmidt Hammer in geomorphological research. Progress in Physical Geography: Earth and Environment, 30(6), 703-718. doi:10.1177/0309133306071954

Goudie, A.S., 2016. Quantification of rock control in geomorphology. Earth-Science Reviews, 159, 374-387. doi:10.1016/j.earscirev.2016.06.012

Hellenic National Meteorological Service, Climate Atlas 1997-2001. Hellenic National Meteorological Service.

Hemelsdaël, R., Ford, M., 2016. Relay zone evolution: a history of repeated fault propagation and linkage, central Corinth rift, Greece. Basin Research, 28(1), 34-56. doi:10.1111/bre.12101

Hijmans, R.J., Cameron, S.E., Parra, J.L., Jones, P.G., Jarvis, A., 2005. Very high resolution interpolated climate surfaces for global land areas. International journal of climatology, 25(15), 1965-1978.

Howard, A.D., Dietrich, W.E., Seidl, M.A., 1994. Modeling fluvial erosion on regional to continental scales. Journal of Geophysical Research: Solid Earth, 99(B7), 13971-13986. doi:10.1029/94jb00744

Hurst, M.D., Mudd, S.M., Yoo, K., Attal, M., Walcott, R., 2013. Influence of lithology on hillslope morphology and response to tectonic forcing in the northern Sierra Nevada of California. Journal of Geophysical Research: Earth Surface, 118(2), 832-851. doi:10.1002/jgrf.20049

Jansen, John D., Codilean, Alexandru T., Bishop, P., Hoey, Trevor B., 2010. Scale Dependence of Lithological Control on Topography: Bedrock Channel Geometry and Catchment Morphometry in Western Scotland. The Journal of Geology, 118(3), 223-246. doi:10.1086/651273

Jansen, J.D., Fabel, D., Bishop, P., Xu, S., Schnabel, C., Codilean, A.T., 2011. Does decreasing paraglacial sediment supply slow knickpoint retreat? Geology, 39(6), 543-546. doi:10.1130/G32018.1

Jungclaus, J.H., Fischer, N., Haak, H., Lohmann, K., Marotzke, J., Matei, D., Mikolajewicz, U., Notz, D., von Storch, J.S., 2013. Characteristics of the ocean simulations in the Max Planck Institute Ocean Model (MPIOM) the ocean component of the MPI-Earth system model. Journal of Advances in Modeling Earth Systems, 5(2), 422-446. doi:10.1002/jame.20023

Kahraman, S., Fener, M., Kozman, E., 2012. Predicting the compressive and tensile strength of rocks from indentation hardness index. Journal of the Southern African Institute of Mining and Metallurgy, 112(5), 331-339.

Kent, E., Boulton, S.J., Whittaker, A.C., Stewart, I.S., Cihat Alçiçek, M., 2017. Normal fault growth and linkage in the Gediz (Alaşehir) Graben, Western Turkey, revealed by transient river long-profiles and slope-break knickpoints. Earth Surface Processes and Landforms, 42(5), 836-852. doi:10.1002/esp.4049

Kirby, E., Whipple, K., 2001. Quantifying differential rock-uplift rates via stream profile analysis. Geology, 29(5), 415-418.

Kirby, E., Whipple, K.X., 2012. Expression of active tectonics in erosional landscapes. Journal of Structural Geology, 44, 54-75. doi:10.1016/j.jsg.2012.07.009
Kontopoulos, N., Doutsos, T., 1985. Sedimentology and tectonic of the Antirion area (western Greece). Bollettino della Societa Geologica Italiana, 104(4), 479-489.
Lavé, J., Avouac, J.P., 2001. Fluvial incision and tectonic uplift across the Himalayas of central Nepal. Journal of Geophysical Research: Solid Earth, 106(B11), 26561-26591. doi:10.1029/2001jb000359
Le Pichon, X., Chamot-Rooke, N., Lallemant, S., Noomen, R., Veis, G., 1995. Geodetic determination of the kinematics of central Greece with respect to Europe: Implications for eastern Mediterranean tectonics. Journal of Geophysical Research: Solid Earth, 100(B7), 12675-12690. doi:10.1029/95jb00317
Leeder, M.R., Mack, G.H., Brasier, A.T., Parrish, R.R., McIntosh, W.C., Andrews, J.E., Duermeijer, C.E., 2008. Late-Pliocene timing of Corinth (Greece) rift-margin fault migration. Earth and Planetary Science Letters, 274(1–2), 132-141. doi:10.1016/j.epsl.2008.07.006
Leopold, L.B., Maddock Jr, T., 1953. The hydraulic geometry of stream channels and some physiographic implications. US Geological Survey Professional Paper, 252, 56.
Maddy, D., 1997. Uplift-driven valley incision and river terrace formation in southern England. Journal of Quaternary Science, 12(6), 539-545. doi:Doi 10.1002/(Sici)1099-1417(199711/12)12:6<539::Aid-Jqs350>3.0.Co;2-T
Manning, R., 1891. On the flow of water in open channels and pipes. Institution of Civil Engineers of Ireland, 20, 161-207.
McNeill, L.C., Collier, R.E.L., 2004. Uplift and slip rates of the eastern Eliki fault segment, Gulf of Corinth, Greece, inferred from Holocene and Pleistocene terraces. Journal of the Geological Society, 161(1), 81-92. doi:10.1144/0016-764903-029
McNeill, L.C., Collier, R.E.L., De Martini, P.M., Pantosti, D., D'Addezio, G., 2005. Recent history of the Eastern Eliki Fault, Gulf of Corinth: geomorphology, palaeoseismology and impact on palaeoenvironments. Geophysical Journal International, 161(1), 154-166. doi:10.1111/j.1365-246X.2005.02559.x
Montgomery, D.R., Gran, K.B., 2001. Downstream variations in the width of bedrock channels. Water Resources Research, 37(6), 1841-1846. doi:10.1029/2000wr900393
Mudd, S.M., Attal, M., Milodowski, D.T., Grieve, S.W.D., Valters, D.A., 2014. A statistical framework to quantify spatial variation in channel gradients using the integral method of channel profile analysis. Journal of Geophysical Research: Earth Surface, 119(2), 138-152. doi:10.1002/2013JF002981
Niedzielski, T., Migoń, P., Placek, A., 2009. A minimum sample size required from Schmidt hammer measurements. Earth Surface Processes and Landforms, 34(13), 1713-1725. doi:10.1002/esp.1851
Nixon, C.W., McNeill, L.C., Bull, J.M., Bell, R.E., Gawthorpe, R.L., Henstock, T.J., Christodoulou, D., Ford, M., Taylor, B., Sakellariou, D., 2016. Rapid spatio-temporal variations in rift structure during development of the Corinth Rift, central Greece. Tectonics, 35, 1225 - 1248. doi:10.1002/2015TC004026
Ori, G.G., 1989. Geologic history of the extensional basin of the Gulf of Corinth (Miocene-Pleistocene), Greece. Geology, 17(10), 918-921. doi:10.1130/0091-7613(1989)017<0918:ghoteb>2.3.co;2
Pechlivanidou, S., Cowie, P.A., Duclaux, G., Nixon, C.W., Gawthorpe, R.L., Salles, T., 2019. Tipping the balance: Shifts in sediment production in an active rift setting. Geology, 47(3), 259-262.
Pechlivanidou, S., Cowie, P.A., Hannisdal, B., Whittaker, A.C., Gawthorpe, R.L., Pennos, C., Riiser, O.S., 2018. Source-to-sink analysis in an active extensional setting: Holocene erosion and deposition in the Sperchios rift, central Greece. Basin Research, 30(3), 522-543. doi:10.1111/bre.12263
Perne, M., Covington, M.D., Thaler, E.A., Myre, J.M., 2017. Steady state, erosional continuity, and the topography of landscapes developed in layered rocks. Earth Surf. Dynam., 5(1), 85-100. doi:10.5194/esurf-5-85-2017
Pirazzoli, P.A., Stiros, S.C., Fontugne, M., Arnold, M., 2004. Holocene and Quaternary uplift in the central part of the southern coast of the Corinth Gulf (Greece). Marine Geology, 212(1–4), 35-44. doi:10.1016/j.margeo.2004.09.006
Roberts, G.G., 2019. Scales of Similarity and Disparity Between Drainage Networks. Geophysical Research Letters, 46(7), 3781-3790. doi:10.1029/2019gl082446
Roberts, G.G., White, N., 2010. Estimating uplift rate histories from river profiles using African examples. Journal of Geophysical Research: Solid Earth, 115(B2).
Rohais, S., Eschard, R., Ford, M., Guillocheau, F., Moretti, I., 2007. Stratigraphic architecture of the Plio-Pleistocene infill of the Corinth Rift: Implications for its structural evolution. Tectonophysics, 440(1-4), 5-28. doi:10.1016/j.tecto.2006.11.006
Roy, S.G., Koons, P.O., Upton, P., Tucker, G.E., 2015. The influence of crustal strength fields on the patterns and rates of fluvial incision. Journal of Geophysical Research: Earth Surface, 120(2), 275-299. doi:10.1002/2014JF003281
Seidl, M., Dietrich, W., 1992. The problem of channel erosion into bedrock. Functional geomorphology, 101-124.
Selby, M., 1980. A rock mass strength classification for geomorphic purposes: with tests from Antarctica and New Zealand. Zeit. fur Geomorph., NF, 24, 31-51.
Sklar, L.S., Dietrich, W.E., 2001. Sediment and rock strength controls on river incision into bedrock. Geology, 29(12), 1087-1090. doi:10.1130/0091-7613(2001)029<1087:sarsco>2.0.co;2
Snyder, N.P., Whipple, K.X., Tucker, G.E., Merritts, D.J., 2003. Channel response to tectonic forcing: field analysis of stream morphology and hydrology in the Mendocino triple junction region, northern California. Geomorphology, 53(1–2), 97-127. doi:10.1016/S0169-555X(02)00349-5
Stark, C.P., 2006. A self-regulating model of bedrock river channel geometry. Geophysical Research Letters, 33(4). doi:10.1029/2005gl023193

Stefatos, A., Papatheodorou, G., Ferentinos, G., Leeder, M., Collier, R., 2002. Seismic reflection imaging of active offshore faults in the Gulf of Corinth: their seismotectonic significance. Basin Research, 14(4), 487-502. doi:10.1046/j.1365-2117.2002.00176.x

Stewart, I., Vita-Finzi, C., 1996. Coastal uplift on active normal faults: The Eliki Fault, Greece. Geophysical Research Letters, 23(14), 1853-1856. doi:10.1029/96GL01595

Stock, J.D., Montgomery, D.R., 1999. Geologic constraints on bedrock river incision using the stream power law. Journal of Geophysical Research. B, 104, 4983-4993.

Sueyoshi, T., Ohgaito, R., Yamamoto, A., Chikamoto, M.O., Hajima, T., Okajima, H., Yoshimori, M., Abe, M., O'Ishi, R., Saito, F., Watanabe, S., Kawamiya, M., Abe-Ouchi, A., 2013. Set-up of the PMIP3 paleoclimate experiments conducted using an Earth system model, MIROC-ESM. Geosci. Model Dev., 6(3), 819-836. doi:10.5194/gmd-6-819-2013

Tucker, G., Lancaster, S., Gasparini, N., Bras, R., 2001. The Channel-Hillslope Integrated Landscape Development Model (CHILD). In: R.S. Harmon, W.W. Doe (Eds.), Landscape Erosion and Evolution Modeling. Springer US, Boston, MA, pp. 349-388. doi:10.1007/978-1-4615-0575-4_12

Tucker, G.E., 2009. Natural experiments in landscape evolution. Earth Surface Processes and Landforms, 34(10), 1450-1460. doi:10.1002/esp.1833

Tucker, G.E., Whipple, K.X., 2002. Topographic outcomes predicted by stream erosion models: Sensitivity analysis and intermodel comparison. Journal of Geophysical Research: Solid Earth, 107(B9), ETG 1-1-ETG 1-16. doi:10.1029/2001jb000162

Viles, H., Goudie, A., Grab, S., Lalley, J., 2011. The use of the Schmidt Hammer and Equotip for rock hardness assessment in geomorphology and heritage science: a comparative analysis. Earth Surface Processes and Landforms, 36(3), 320-333. doi:10.1002/esp.2040

Watkins, S.E., Whittaker, A.C., Bell, R.E., McNeill, L.C., Gawthorpe, R.L., Brooke, S.A.S., Nixon, C.W., 2018. Are landscapes buffered to high-frequency climate change? A comparison of sediment fluxes and depositional volumes in the Corinth Rift, central Greece, over the past 130 k.y. GSA Bulletin, 131(3-4), 372-388. doi:10.1130/b31953.1

Westaway, R., Guillou, H., Yurtmen, S., Beck, A., Bridgland, D., Demir, T., Scaillet, S., Rowbotham, G., 2006. Late Cenozoic uplift of western Turkey: Improved dating of the Kula Quaternary volcanic field and numerical modelling of the Gediz River terrace staircase. Global and Planetary Change, 51(3), 131-171. doi:10.1016/j.gloplacha.2006.02.001

Whipple, K.X., Snyder, N.P., Dollenmayer, K., 2000. Rates and processes of bedrock incision by the Upper Ukak River since the 1912 Novarupta ash flow in the Valley of Ten Thousand Smokes, Alaska. Geology, 28(9), 835-838.

Whipple, K.X., Tucker, G.E., 1999. Dynamics of the stream-power river incision model: Implications for height limits of mountain ranges, landscape response timescales, and research needs. Journal of Geophysical Research: Solid Earth, 104(B8), 17661-17674. doi:10.1029/1999jb900120

Whipple, K.X., Tucker, G.E., 2002. Implications of sediment-flux-dependent river incision models for landscape evolution. Journal of Geophysical Research: Solid Earth, 107(B2), ETG 3-1-ETG 3-20. doi:10.1029/2000JB000044

Whittaker, A.C., Attal, M., Cowie, P.A., Tucker, G.E., Roberts, G., 2008. Decoding temporal and spatial patterns of fault uplift using transient river long profiles. Geomorphology, 100(3-4), 506-526. doi:10.1016/j.geomorph.2008.01.018

Whittaker, A.C., Boulton, S.J., 2012. Tectonic and climatic controls on knickpoint retreat rates and landscape response times. Journal of Geophysical Research: Earth Surface, 117(F2).

Whittaker, A.C., Cowie, P.A., Attal, M., Tucker, G.E., Roberts, G.P., 2007a. Bedrock channel adjustment to tectonic forcing: Implications for predicting river incision rates. Geology, 35(2), 103-106. doi:10.1130/g23106a.1

Whittaker, A.C., Cowie, P.A., Attal, M., Tucker, G.E., Roberts, G.P., 2007b. Contrasting transient and steady-state rivers crossing active normal faults: new field observations from the Central Apennines, Italy. Basin Research, 19(4), 529-556. doi:10.1111/j.1365-2117.2007.00337.x

Wobus, C., Whipple, K.X., Kirby, E., Snyder, N., Johnson, J., Spyropolou, K., Crosby, B., Sheehan, D., 2006. Tectonics from topography: Procedures, promise, and pitfalls. Geological Society of America Special Papers, 398, 55-74. doi:10.1130/2006.2398(04)

Wohl, E.E., Merritt, D.M., 2001. Bedrock channel morphology. Geological Society of America Bulletin, 113(9), 1205-1212.

Yagiz, S., 2009. Predicting uniaxial compressive strength, modulus of elasticity and index properties of rocks using the Schmidt hammer. Bulletin of Engineering Geology and the Environment, 68(1), 55-63. doi:10.1007/s10064-008-0172-z

Yanites, B.J., Becker, J.K., Madritsch, H., Schnellmann, M., Ehlers, T.A., 2017. Lithologic Effects on Landscape Response to Base Level Changes: A Modeling Study in the Context of the Eastern Jura Mountains, Switzerland. Journal of Geophysical Research: Earth Surface, 122(11), 2196-2222. doi:10.1002/2016jf004101

Zagorchev, I., 2007. Late Cenozoic development of the Strouma and Mesta fluviolacustrine systems, SW Bulgaria and northern Greece. Quaternary Science Reviews, 26(22), 2783-2800. doi:10.1016/j.quascirev.2007.07.017

Ford, M., Rohais, S., Williams, E.A., Bourlange, S., Jousselin, D., Backert, N., Malartre, F., 2013. Tectono-sedimentary evolution of the western Corinth rift (Central Greece). Basin Research, 25(1), 3-25. doi:10.1111/j.1365-2117.2012.00550.x

Ghisetti, F., Vezzani, L., 2005. Inherited structural controls on normal fault architecture in the Gulf of Corinth (Greece). Tectonics, 24(4). doi:10.1029/2004tc001696

Nixon, C.W., McNeill, L.C., Bull, J.M., Bell, R.E., Gawthorpe, R.L., Henstock, T.J., Christodoulou, D., Ford, M., Taylor, B., Sakellariou, D., 2016. Rapid spatio-temporal variations in rift structure during development of the Corinth Rift, central Greece. Tectonics, 35, 1225 - 1248. doi:10.1002/2015TC004026

Rohais, S., Eschard, R., Ford, M., Guillocheau, F., Moretti, I., 2007. Stratigraphic architecture of the Plio-Pleistocene infill of the Corinth Rift: Implications for its structural evolution. Tectonophysics, 440(1-4), 5-28. doi:10.1016/j.tecto.2006.11.006